metals

MDPI

Review

Advances in Understanding the Evolution Mechanism of Micropore Defects in Metal Materials under External Loads

Jianwei Liang [1,2], Menghao Zhang [1], Yan Peng [1,2] and Jiapo Wang [1,2,3,*]

[1] School of Mechanical Engineering, Yanshan University, Qinhuangdao 066004, China
[2] National Engineering Research Center for Equipment and Technology of Cold Strip Rolling, School of Mechanical Engineering, Yanshan University, Qinhuangdao 066004, China
[3] Hebei Light Structural Equipment Design and Manufacturing Technology Innovation Center, Yanshan University, Qinhuangdao 066004, China
* Correspondence: jpwang@ysu.edu.cn or jpwang@mail.nwpu.edu.cn

Abstract: Micropores are one of the critical factors affecting materials' performance and service life. As the need for a deeper understanding of micropore evolution and damage mechanisms grows, assessing the mechanical properties of materials containing micropores and predicting the lifespan of related metal structural components becomes increasingly complex. This paper focuses on the evolution process, regularities, and research methods of micropores in metal materials. Based on recent research and practical applications, the key stages of micropore evolution are discussed, encompassing nucleation, growth, coalescence, collapse, interaction, and the influence of other microstructures. Firstly, the advantages and limitations of commonly used characterization methods such as scanning electron microscopy, transmission electron microscopy, and X-ray computed tomography are introduced in the study of micropore evolution. Subsequently, critical theoretical models for micropore evolution, such as the Gurson model and its extensions, are summarized. By using a multiscale approach combining the crystal plasticity finite element method, dislocation dynamics, and molecular dynamics, the factors influencing the micropore evolution, such as external stress conditions, internal microstructures, and micropore characteristics, are specifically elaborated, and the basic physical mechanisms of micropore evolution are analyzed. Finally, a comprehensive review and summary of current research trends and key findings are provided, and a forward-looking perspective on future research directions is presented.

Keywords: micropore evolution; pore damages; mechanical property

Citation: Liang, J.; Zhang, M.; Peng, Y.; Wang, J. Advances in Understanding the Evolution Mechanism of Micropore Defects in Metal Materials under External Loads. *Metals* **2024**, *14*, 522. https://doi.org/10.3390/met14050522

Received: 11 April 2024
Revised: 22 April 2024
Accepted: 24 April 2024
Published: 29 April 2024

1. Introduction

Metal materials, such as nickel, titanium, aluminum, etc., are widely used in various industries due to their excellent mechanical properties, including marine transportation, aviation, agricultural machinery, and other fields. Metal materials undergo different types of damage during service life, with fatigue fracture, wear, and corrosion emerging as the predominant degradation modes. Fatigue fracture stands out as the most prevalent form of failure. In the metal materials molding process, technical constraints frequently result in the formation of defects such as inclusions, orientation deviations, and micropores. Micropores refer to tiny spaces or pore structures at the nanometer to micrometer scale, usually caused by defects, gas, stress concentration, dislocation movement, etc., within the material. They can significantly impact the mechanical properties, fatigue life, corrosion resistance, and other properties of materials. The size of micropores typically ranges from a few nanometers to several micrometers. It can be observed under high-resolution microscopes such as metallographic microscopes, transmission electron microscopes, and industrial X-ray computed tomography (XCT) scans.

For example, in the casting process, micropores can form when the gases generated during the solidification of molten metal are not efficiently vented. Furthermore, the insufficient replenishment of molten metal due to volume shrinkage during the solidification stage may lead to the formation of shrinkage micropores. Irregularities in composition within the grains can result in segregation, and micropores may occur due to plastic changes between inclusion particles and matrix particles [1]. Additionally, during the heat treatment or processing of metal materials, issues such as excessive burning, expansion, and delamination may occur, adversely affecting material properties and leading to the formation of micropores. Throughout casting and heat treatment processes, current technology inevitably leads to defects such as micropores and microcracks in metal materials [2]. Subsequently, this leads to considerable changes in the material's mechanical properties, especially the emergence of complex morphological micropores, which pose a challenge to evaluating the mechanical properties.

Moreover, new micropores can form when metal materials are subjected to service loads. The mechanisms and processes of pore formation determine the shape of the micropores. Inside grains, pores are typically spherical or approximately spherical, while pores formed near grain boundaries or around dislocations may exhibit irregular shapes.

Micropores are prevalent in metallic materials, encompassing nickel-based single-crystal superalloys for aero-engine turbine blades, high-strength and high-toughness special steel, titanium alloys, cast aluminum alloys, and additive manufacturing polycrystalline (as shown in Figure 1). Micropores, in particular, can significantly impact the utilization rate, yield of finished products, overall performance, and production efficiency of these materials, having a profound effect on the fatigue life of ductile metal materials [3]. They have emerged as a critical issue leading to performance degradation during metal materials' preparation, subsequent processing, and service life. As a result, comprehensively evaluating the mechanical characteristics of metal materials with micropores in complex service environments and forecasting the lifespan of associated metal structural components becomes increasingly challenging. The morphological changes that occur during the evolution of micropores lead to a stress concentration around the pores, triggering premature material failure and significant losses. Therefore, a comprehensive assessment of the mechanical properties of metal materials in complex operating environments and the prediction of the lifespan of the related metal structural components must consider the impact of morphological changes during the evolution of micropores.

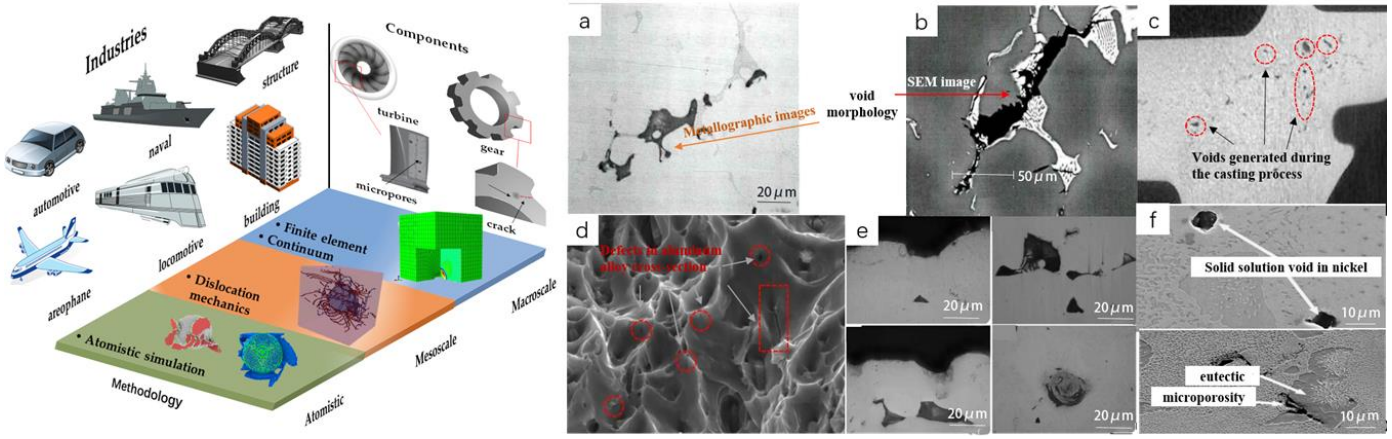

Figure 1. Micropores' critical role and characterization in various metals: (**a**) GW63K magnesium [4]; (**b**) GW63K magnesium [4]; (**c**) ductile iron [5]; (**d**) aluminum [6]; (**e**) TC4 titanium [7]; (**f**) nickel single crystal [8]. Reprinted from ref. [4–8]; 2024 University of Science and Technology of China, Foundry Technology, General Institute of Mechanical Science Research, Shenyang Aerospace University.

Nickel-based single-crystal turbine blades in aerospace engines serve as a representative example. Beyond common defects such as impurities, freckles, orientation deviations,

and minor misalignments, micropores have emerged as a critical factor influencing the mechanical properties of nickel-based single-crystal alloys [3,9]. After experiencing an overtemperature or overload, micropores in aero-engine turbine blades undergo significant changes when subjected to thermal shock loads. This process initiates micro-damage in the nickel-based single-crystal material. Scanning electron microscopy (SEM) observations illustrate the substantial impact of micropores on the material's performance, leading to the formation of initial microcracks due to interactions among these micropores [10]. Micropores' nucleation, growth, and coalescence are widely considered as the primary factors contributing to material fracture failure [11–13]. Since micropores are inevitable, their presence significantly influences the plastic deformation mechanism of the material.

Hot isostatic pressing (HIP) technology alleviates micropore-related issues in materials and diminishes their adverse effects on material properties. In metal material processing, only one or two directions can usually be applied with pressure to the material simultaneously to obtain a dense product. However, equal pressure can be applied to the material from all directions during the HIP process to achieve a more compact product. The material undergoes high temperatures and high-pressure conditions, causing plastic deformation and the collapse of micropore regions, which reduces micropore volume, promoting diffusion and bonding between the micropore walls and the surrounding material.

Consequently, porosity decreases, improving material density and enhancing mechanical properties. While HIP effectively mitigates micropores to some extent, it is crucial to note that the complete elimination of micropores is unattainable [14–16]. Therefore, further research into the evolution of micropores in operational environments is essential to enhance the understanding of their impact on material performance. Various studies, utilizing both experimental and simulation methods, have been undertaken to better characterize the ductile fracture process, with a focus on the evolution of micropores. Typically, the traditional method for studying micropores involves subjecting material samples to tensile, fatigue, or creep experiments to simulate natural working conditions. These tests are then halted at the critical deformation stage, and the cross-section of the sample is scrutinized using equipment such as an SEM or a transmission electron microscope (TEM). Image processing extracts two-dimensional (2D) plane information about the micropores [11–13,17–21]. SEM and TEM observations have inherent limitations, as they are restricted to capturing specific time points and cannot trace the dynamic evolution of micropores over time.

Furthermore, the observation process in these techniques may damage the material, introducing the possibility of errors in the obtained results [22]. The in-situ SEM/TEM techniques developed on top of SEM/TEM technologies enable researchers to directly observe the deformation, fracture, phase transformation, and other processes of materials during loading, which is essential for studying the failure mechanisms, phase transformation behaviors, lattice distortions, and other aspects of materials. However, employing 2D characterization methods proves inadequate for comprehensively capturing micropores' complete three-dimensional (3D) attributes, especially their intricate morphology, spatial distribution, and porosity, leading to significant biases in the results [23].

XCT studies have unveiled the connectivity of certain neighboring micropores observed in 2D metallography, indicating a three-dimensional interconnection. This finding implies that relying solely on 2D analyses derived from cross-sectional views may lead to the underestimation of micropore quantity and a reduction in their apparent size and morphological intricacy [24]. XCT provides the capability to non-destructively visualize the spatial morphology of micropores within a material, offering a clear and undistorted representation of their spatial characteristics. In our research on the evolution of micropores in nickel-based single-crystal superalloys, our research group has obtained two-dimensional and three-dimensional views of micropores in the material using XCT. Additionally, we have successfully obtained information regarding these micropores' size, shape, and location, enabling the non-destructive detection of micropore information within the material. The detection results are presented in Figure 2.

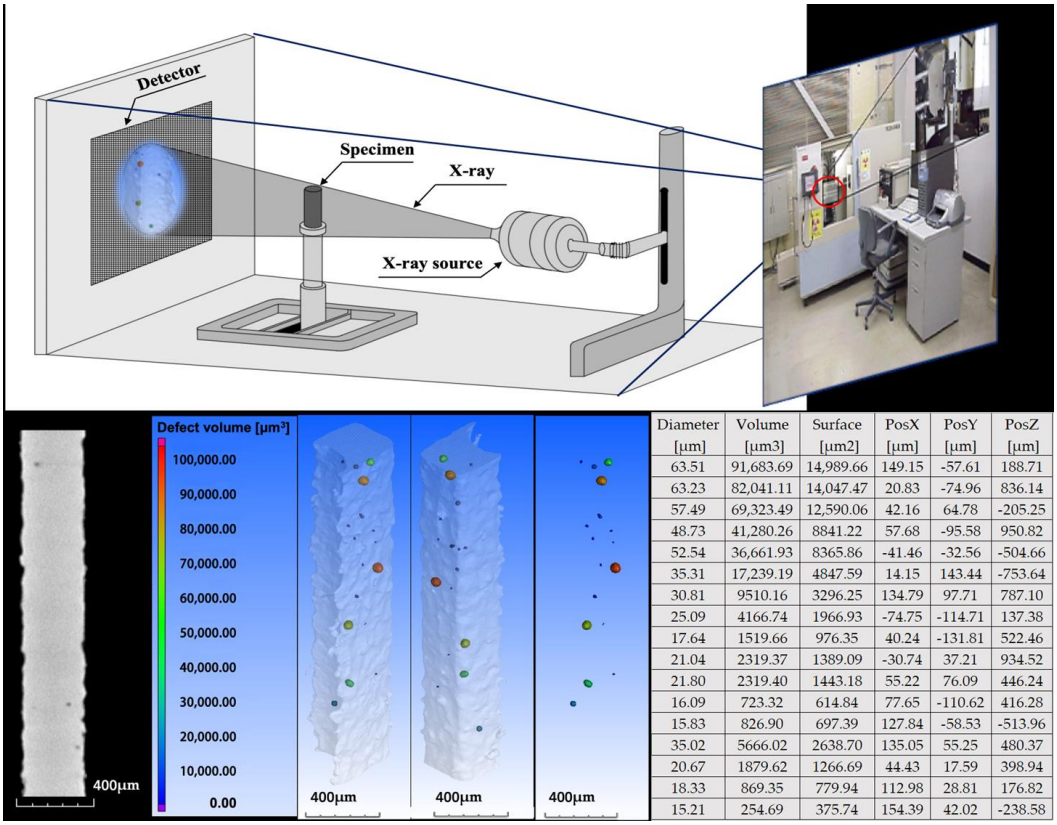

Diameter [μm]	Volume [μm3]	Surface [μm2]	PosX [μm]	PosY [μm]	PosZ [μm]
63.51	91,683.69	14,989.66	149.15	-57.61	188.71
63.23	82,041.11	14,047.47	20.83	-74.96	836.14
57.49	69,323.49	12,590.06	42.16	64.78	-205.25
48.73	41,280.26	8841.22	57.68	-95.58	950.82
52.54	36,661.93	8365.86	-41.46	-32.56	-504.66
35.31	17,239.19	4847.59	14.15	143.44	-753.64
30.81	9510.16	3296.25	134.79	97.71	787.10
25.09	4166.74	1966.93	-74.75	-114.71	137.38
17.64	1519.66	976.35	40.24	-131.81	522.46
21.04	2319.37	1389.09	-30.74	37.21	934.52
21.80	2319.40	1443.18	55.22	76.09	446.24
16.09	723.32	614.84	77.65	-110.62	416.28
15.83	826.90	697.39	127.84	-58.53	-513.96
35.02	5666.02	2638.70	135.05	55.25	480.37
20.67	1879.62	1266.69	44.43	17.59	398.94
18.33	869.35	779.94	112.98	28.81	176.82
15.21	254.69	375.74	154.39	42.02	-238.58

Figure 2. The XCT examination results of micropores in nickelbased singlecrystal alloys.

XCT has obtained a large amount of data and three-dimensional information on micropores in materials, allowing us to professionally transform this data and three-dimensional information into geometric models that better approximate the geometric information of micropores in actual materials. While these geometric models prove useful for subsequent finite element simulations, the observation of micropore evolution from a three-dimensional perspective is still under investigation. In recent years, significant progress has been made in the study of micropore evolution thanks to advancements in in-situ observation equipment using XCT [25–33], which allows for observing micropore evolution during experiments, contributing to a more detailed and precise understanding of the process [24]. Chen et al. [34] used in situ XCT to observe micropores' nucleation and growth behavior during the tensile deformation process of dual-phase steel, quantifying the changes in pore quantity and porosity during pore evolution. Similarly, Zhang et al. [35] also utilized in situ XCT to reconstruct a three-dimensional visualization model of low-carbon steel, quantitatively analyzing the characteristics of micro-pore evolution from a three-dimensional perspective. The characterization results are shown in Figure 3. Visualizing the three-dimensional evolution process of micropores is a unique advantage of in situ XCT. It is expected to play a significant role in future research on micropore evolution.

Nevertheless, more than relying solely on experimental observations is required for a comprehensive analysis of the evolution behavior and damage effects of micropores. Advanced numerical simulation methods such as dislocation dynamics (DD) [36–43] and molecular dynamics (MD) [44–52] are used to elucidate the evolutionary mechanism of micropores. The crystal plastic finite element method (CPFEM) [53–64], employing XCT for three-dimensional micropore reconstruction, is used to investigate the correlation between micropores' 3D characteristics and the mechanical behavior of materials. However, accurately describing the evolutionary mechanism of micropores proves to be challenging using this approach. The CPFEM faces challenges in accurately characterizing nonlinear behaviors, including phase transformation, phase boundary transformation, and fracture,

in materials undergoing significant deformation and complex loading conditions. This limitation stems from CPFEM's reliance on assumptions about the microstructure evolution process, assuming a uniform distribution of dislocation density and strain within the crystal. Moreover, it solely accounts for the elastic and plastic behavior of the material, neglecting crucial processes such as dislocation generation and destruction, along with interactions between microstructures like grain boundaries and twins. Consequently, a comprehensive understanding of the microstructure evolution mechanism remains constrained, and depending solely on the CPFEM may not provide precise results. Researchers have progressively integrated the CPFEM with DD and MD to address these challenges to form a multiscale model. DD simulations offer intricate details about dislocation activities and distributions. By simulating dislocation dynamics, the motion and interactions of dislocations can be scrutinized, revealing the plastic behavior and microstructure evolution mechanisms of crystals. Furthermore, MD simulations can model the behavior of crystals at the atomic level, capturing interactions between atoms. Through MD simulations, crystals' atomic structure and dynamic behavior can be investigated, providing precise input parameters for the CPFEM. This multiscale method offers an effective method for analyzing the plastic behavior and microstructure evolution mechanisms of materials, making it a crucial direction in advancing research on the evolution of micropores. For example, Niu et al. [65] proposed toughness fracture criteria related to micropore nucleation, growth, and coalescence by utilizing a multiscale model combining finite element analysis with molecular dynamics. Of course, multiscale models are wider than the three methods mentioned above. They also include phenomenological models that summarize objective phenomena and advanced numerical simulation methods.

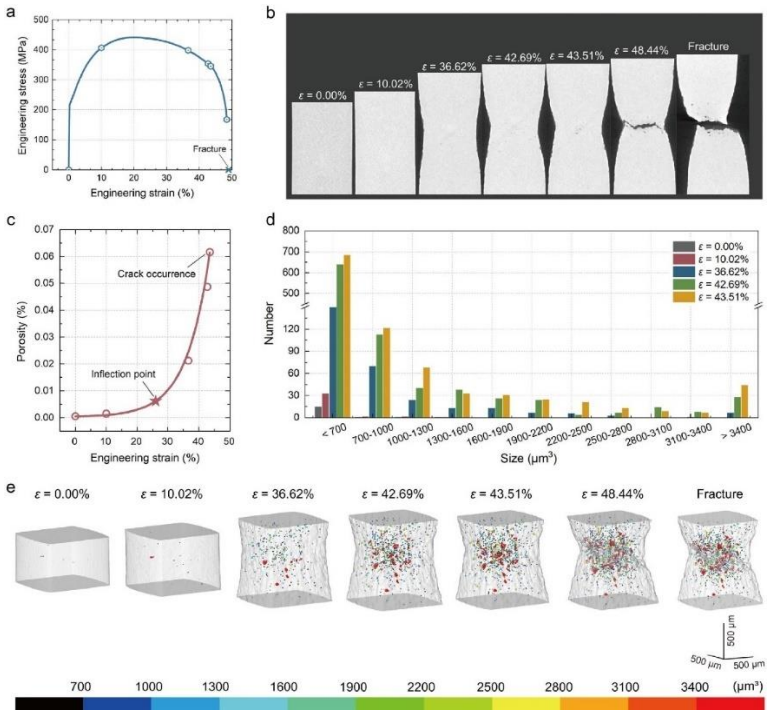

Figure 3. In situ XCT characterization of the evolution process of micropores in low carbon steel [35]. (**a**) Engineering stress versus engineering strain curve; (**b**) Sequence of 2D X-ray tomography images at different strain levels; (**c**) Porosity versus engineering strain curve; (**d**) Size distribution of pores at various strain levels; (**e**) 3D spatial distribution of pores in selected central region at different strain levels. Reprinted with permission from ref. [35]; 2023 Engineering Fracture Mechanics.

To comprehensively depict the research progress and potential development in micropore-related fields, this article conducts a detailed review of various aspects of micropore evolution, as shown in Figure 4. This encompasses micropore nucleation, growth, collapse,

interference, coalescence, and interaction with other microstructural elements. This article outlines research methods for studying micropore evolution, organizes the theoretical model of micropore evolution, categorizes the main mechanical properties affected by micropores, and discusses the atomic-level complexity and manifestations of micropore evolution. The purpose is to clarify the fundamental physical principles governing the complex micropore evolution process described above. Additionally, this article addresses the limitations of current micropore research and provides insights into future directions and emerging trends in the field.

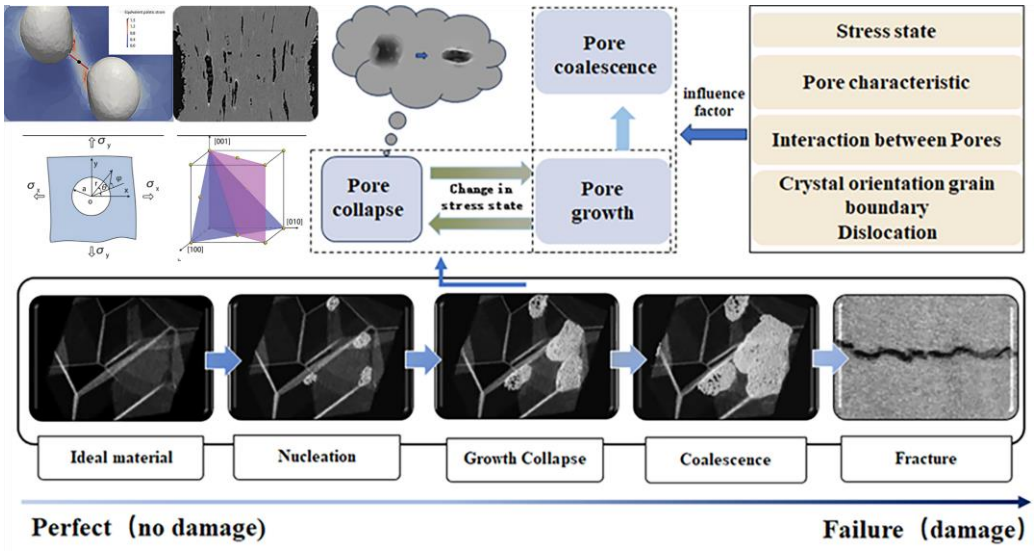

Figure 4. Micropores' damage process and influencing factors: a comprehensive review.

2. Nucleation Causes and Principles

Among the failure mechanisms observed in ductile metals, micropore nucleation remains the least understood, primarily due to its occurrence at microscopic or even nanoscale levels, presenting challenges for direct observation and study. The nucleation of micropores results from damage induced by external factors, including loading and temperature variations. In experiments conducted by Pathak et al. [66], high-strength steels DP780 and CP800 were utilized. Their analysis unveiled a direct connection between micropore nucleation and macroscopic stress states. Particularly noteworthy was the observation that CP800 steel exhibited a higher nucleation strain and a faster micropore nucleation rate than DP780 steel under identical conditions, emphasizing the critical role of stress state as a determining factor in micropore nucleation. Therefore, the influence of the stress state on micropore nucleation has been a central focus of the investigation, emphasizing a correlation between the mechanism of micropore nucleation and stress triaxiality. The critical strain for micropore nucleation depends on stress triaxiality [67]. Furthermore, the inherent properties of materials serve as the fundamental influencing factors for micropore nucleation. To comprehensively grasp the micropore nucleation mechanism, it is crucial to take into account the material's microstructure.

In previous research, the nucleation of micropores in various material mediums, including uniformly elastic, perfectly plastic, nonlinearly elastic, and power-law hardening materials, has been interpreted as a cavitation instability phenomenon [68,69]. Currently, the nucleation of micropores is widely believed to be closely linked to second-phase particles [53,64,70–77]. Encountering at least two distinct phase structures or other inclusion particles in metallic materials is commonplace. Based on extensive experimental observations, two primary mechanisms for micropore nucleation have been summarized: stress nucleation and deformation nucleation [78–81]. Stress nucleation occurs when the interphase structures separate or when the phase structures themselves undergo destruction because the interface stress surpasses critical threshold stress. Deformation nucleation is

linked to separating the phase structure/matrix interface when the equivalent plastic strain attains a critical value, following the dislocation accumulation model.

Subsequent microscopic investigations have put forth various hypotheses regarding nucleation, as shown in Figure 5. Firstly, micropores are thought to originate from the interaction of edge dislocations and external impact forces. Secondly, stress accumulation and subsequent nucleation of micropores can occur in regions where the slip zone intersects grain boundaries or various defects, a phenomenon known as the Zener–Stroh mechanism [82]. Thirdly, when the material undergoes applied plastic strain, it can experience vacancy supersaturation. Unless the vacancies are stabilized through the trapping of interstitial gases or the application of hydrostatic stress, they will collapse to form planar defects when their size exceeds the critical limit of 10 vacancies [83–87]. Lastly, due to the presence of second-phase particles or inclusions within the matrix, and the consistency of inclusions with the matrix is usually lower than the consistency of the material itself, the nucleation of pores is induced [88,89].

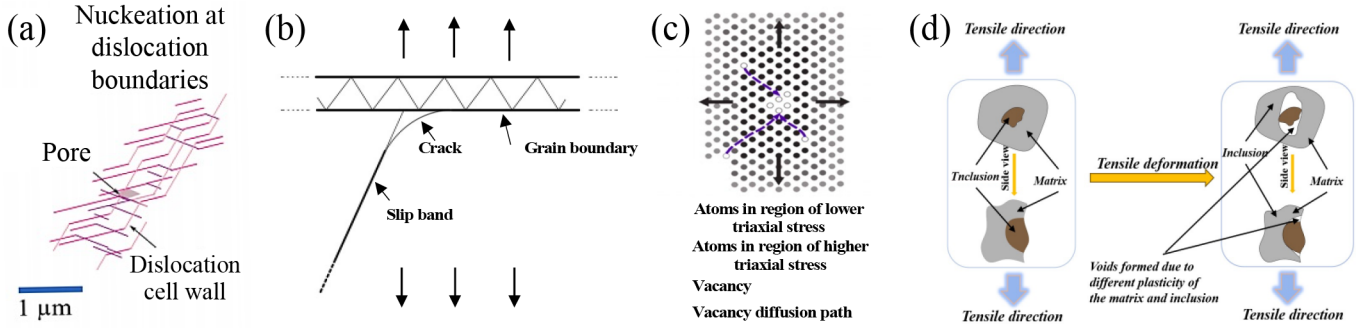

Figure 5. Micropore nucleation mechanisms [89]; (**a**) dislocation interaction; (**b**) dislocations accumulate at grain boundaries; (**c**) vacancy coalescence; (**d**) loss of inclusions to the matrix. Reprinted with permission from ref. [89]; 2023 Progress in Materials Science.

Differences in microstructure among various metallic materials lead to variations in the nucleation mechanisms of micropores. Nevertheless, a consensus has been reached regarding the probable nucleation sites of micropores, typically found in the weaker regions within the material. Micropores tend to nucleate at joints and interfaces, including defects, grain boundaries, and phase interfaces. These regions disrupt the continuity and integrity of the material's microstructure, leading to substantial dislocation accumulation and stress concentration. This, in turn, can induce local deformation and facilitate micropore nucleation. Recent advancements in testing technologies, such as SEM, TEM, and XCT, have facilitated the direct observation of the micropore nucleation mechanisms mentioned. However, these techniques are restricted to observing the evolution of micropores as they grow to a sufficient size. More advanced microscopic characterization equipment and techniques are required to investigate micropores' initial formation and early evolution occurring at more minor scales. Additionally, complementary microscale theoretical calculation methods, such as DD and MD, become essential for a more comprehensive understanding of these processes.

In particular, MD simulations are crucial in offering a more comprehensive atomic-scale perspective for studying micropore nucleation mechanisms. Zhao et al. conducted MD simulations to investigate micropore nucleation in an ideal lattice exposed to static water tension [90]. Their results indicated that plasticity must commence before uniform micropore nucleation. Moreover, they also considered the influence of hydrogen on micropore nucleation and developed a relevant mathematical model. This work lays the theoretical groundwork and provides novel insights for the research and development of hydrogen storage materials and equipment. Yang et al. utilized MD simulations to investigate the effects of temperature, strain rate, initial pressure, and grain size on micropore nucleation under both isotropic and triaxial stress conditions [91]. The advancement of precision

equipment, nuclear industries, and advanced manufacturing has substantially expanded the application scope of metal materials, elevating the significance of micropore defects in these materials. Understanding the mechanisms of micropore nucleation has become a pressing need, yet characterizing and observing these details using existing techniques remains challenging. Consequently, there is an urgent demand to develop micro-nano mechanics theory and conduct further research on dislocation and atomic scales to address this issue.

3. Growth Law and Research Methods

Micropore growth is a crucial aspect of material damage, signifying a non-uniform plastic deformation process that persists over an extended period during micropore evolution. Consequently, existing research on micropore evolution predominantly centers on the growth of these micropores. Factors influencing the micropores' growth can be primarily categorized into the following three groups, as shown in Figure 6: external stress conditions [53,92–95] (stress triaxiality, Lode parameter), internal microstructure [61,63,96–101] (such as grain orientation, grain size, etc.), and micropores' characteristics [31,53,102–105] (such as initial micropore volume, micropore size, shape, etc.).

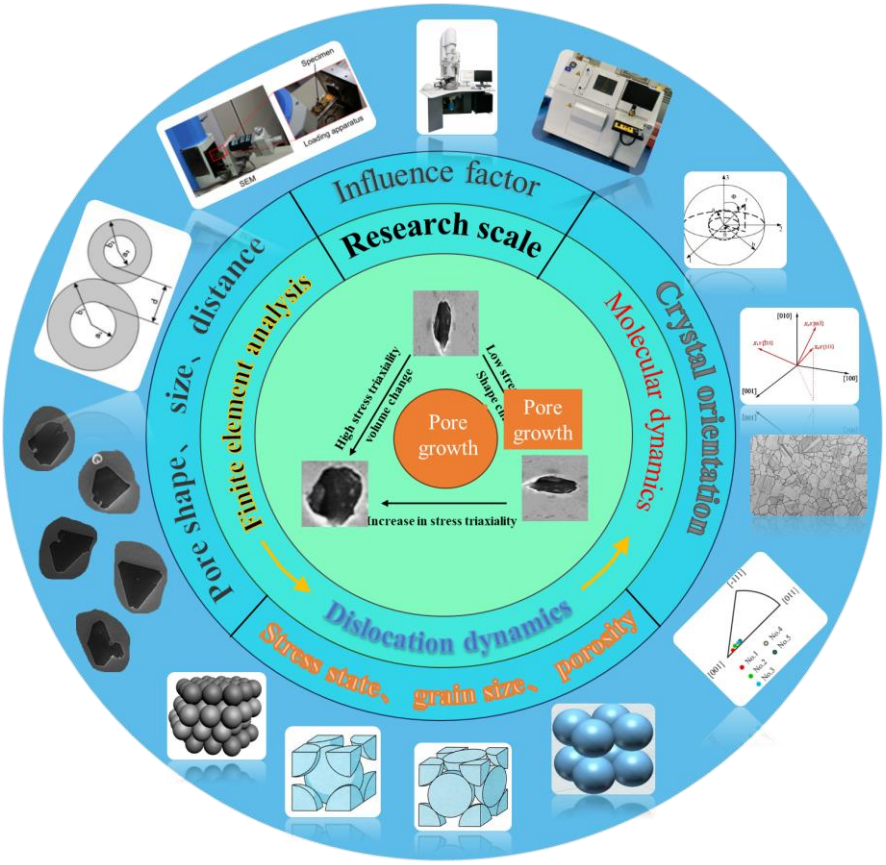

Figure 6. Overview of pore growth research.

Research on micropore growth has emerged from the understanding that micropore evolution significantly influences ductile material damage. Initially, studies concentrated on the growth of micropores in an infinite elastic solid with a single micropore, assuming a round or spherical shape for the micropore. Subsequent research investigated the growth of micropores with multiple cylindrical holes, considering the interaction between adjacent micropores. It is apparent that these models still exhibit notable gaps and limitations when compared to the actual micropores in materials. Further studies are incorporating the evolution of porosity into the constitutive equation and considering material damage within

a plastic constitutive framework. Presently, numerous models utilize this methodology to examine micropore growth, with the Gurson model [106] and its extended models among the most classic models in this category.

Mandel [107] and Hill [108] pioneered the standard method of homogenization theory, coupling the representative volume elements of the microstructure with the macroscopic ones through volume averaging. Subsequently, Gurson [109], based on the von Mises solid matrix with a hollow sphere model under uniform boundary strain rate conditions, proposed a micro–macro limit analysis method. Gurson established the classic Gurson model by introducing a ductile yield criterion and flow law for porous ductile materials based on damage mechanisms. The original Gurson model assumes isotropic strain hardening locally by combining plasticity theory with the homogenization of "basic units" in plastic porous materials. It overlooks the influence of internal microstructure, such as crystal orientation, and treats the pure tensile yield stress of the material as constant. They have promoted research in the field of pore growth. However, Gurson's analysis utilized the kinematic limit analysis approach to obtain an upper bound on the macroscopic criterion for spherical porous materials. As a result, this model tends to overestimate material strength and underestimate material porosity due to the restriction on pore growth.

The original Gurson criterion has undergone multiple extensions, with one of the most notable being the introduction of three additional calibration parameters q_1 q_2 q_3 by Tvergaard to enhance the consistency between the Gurson yield criterion predictions and experimental data [110]. Tvergaard also proposed a widely used pore coalescence method within this framework, leading to the Gurson–Tvergaard–Needleman (GTN) model. Tvergaard suggested $q_1 = 1.5$, $q_2 = 1$, $q_3 = q_1^2$, but later, Koplik and Needleman [111] pointed out that the values of q_i are not fixed and are arbitrary parameters that ensure the correlation between equivalent plastic strain and pore growth, influenced by the stress triaxiality T. However, Tvergaard's suggested values still hold some merit. In the 1980s, Tvergaard, Needleman, and others introduced additional terms related to micropore nucleation to incorporate porosity into yield criteria and associated flow rules [110,112–116].

The cubic sphere pore model may undergo shear yielding under low-stress conditions, which the Gurson model cannot predict. Therefore, Hom et al. [117] also proposed a modified form of the Gurson yield criterion. Later, Leblond [118] derived another yield function in analyzing representative volume elements with spherical pores and proposed a pore growth model related to shear, known as the Leblond–Perrin–Devaux (LPD) model. This model overcomes some limitations of the Gurson model: (1) the Gurson model cannot simultaneously determine the yield stress of the hardening matrix under pure shear and pure tensile stress with the same accuracy, (2) the Gurson model's predictions are incompatible with analytical solutions for a hollow sphere made of rigid hardening material under tensile stress, and (3) the Gurson model cannot reproduce the relationship between pore growth rate and matrix hardening function [119].

The models mentioned above are limited to analyzing spherical pores. Gologanu and others [120], as well as Castañeda et al. [121], have proposed constitutive models that incorporate changes in pore shape. Gologanu and colleagues used micromechanical analysis to study pores in elongated and flattened spheres [122], considering the influence of the aspect ratio of the pores. They extended the Gurson model, now commonly called the Gologanu–Leblond–Devaux (GLD) model.

Additionally, Mear, Hutchinson (1985), and Leblond (1995) have significantly advanced the extension of the Gurson model, enhancing the accuracy of pore growth predictions [118,123]. Numerous extensions and modifications to the Gurson model have been proposed, including incorporating Eshelby-type velocity fields in the limit analysis of hollow spheres and considering a matrix that follows Tresca's criterion instead of von Mises' [124]. Due to space limitations, mentioning all these variants in this article is impossible. The descriptions of some relevant models are provided in Table 1. The meanings of the parameters in Table 1 are shown in Table 2

Table 1. Introduction to some micropore growth models.

Model	Equation	Description
Gurson model 1977	$\Phi(\sigma, f_v) = \frac{\sigma_{eq}^2}{\sigma_0^2} + 2f_v \cosh(\frac{3\Sigma_h}{2\sigma_0}) - 1 - f_v^2 = 0$ Changes in porosity during the plastic deformation process: $\dot{f}_v = \frac{d}{dt}(\frac{\omega}{\Omega}) = (1 - \frac{\omega}{\Omega})\frac{\dot{\Omega}}{\Omega}$ or $\dot{f}_v = (1 - f_v)\mathbf{tr}\mathbf{D}^p$ Changes in porosity during the elastic deformation process: $f_v = 1 - (1 - f_{v0})\frac{V_0}{V}\left[1 + \frac{3(1-2v)}{E}\Sigma_h\right]$	The earliest pore growth model based on a plastic constitutive framework only considers spherical pores and material isotropy.
GTN model 1980, 1981	$\frac{\sigma_{eq}^2}{\sigma_e^2} + 2q_1 f_v^* \cosh(\frac{3q_2\Sigma_h}{2\sigma_e}) - 1 - q_3 f_v^{*2} = 0$ $f_v^*(f_v) = \begin{cases} f_v, f_v \le f_{vC} \\ f_{vC} + \frac{f_{vU} - f_{vC}}{f_{vF} - f_{vC}}, f_v > f_{vC} \end{cases}$	Extension of the Gurson model: To enhance the consistency between the Gurson yield criterion predictions and experimental data, three additional calibration parameters $q_i (i = 1, 2, 3)$ have been incorporated into the structure of the criterion. Furthermore, a widely adopted pore clustering method has been proposed.
LPD model 2006	$\frac{\sigma_{eq}^2}{\sigma_{e1}^2} + 2q_1 f_v^* \cosh(\frac{\ln(q_1 f_v^*)}{\ln(f_v)} \frac{3q_2\Sigma_h}{2\sigma_{e2}})$ $-1 - q_3 f_v^{*2} = 0$ $\sigma_{e1} = \frac{1}{b^3 - a^3}\int_{a^3}^{b^3} \sigma_e(\langle\varepsilon_e^r\rangle_r) dr^3$ $\sigma_{e2} = \frac{1}{\ln(b^3/a^3)}\int_{a^3}^{b^3} \sigma_e(\langle\varepsilon_e^r\rangle_r) \frac{dr^3}{r^3}$ $\langle\varepsilon_e^r\rangle_r = \frac{2}{3}\left[\sinh^{-1}(u) - \frac{\sqrt{1+u^2}}{u}\right]_{u=\frac{2}{3}E_{kk}^p/(E_{eq}^p r^3)}^{u=\frac{2}{3}E_{kk}^p/(E_{eq}^p R^3)}$ $b^3 = \exp(E_{kk}^p), a^3 = \exp(E_{kk}^p) - f_{v0} - 1$ $R^3 = r^3 - b^3 = 1$	Incorporating a correction factor to account for the overestimation of pore growth in the Gurson model under shear loading.
GLD model 1995	$C^*\left(\frac{\Sigma_z - \Sigma_r + \eta\Sigma_h}{\sigma_e}\right) + 2q(g+1)(g+f_v)$ $\cosh\left(k\frac{\Sigma_h}{\sigma_e}\right) - (g+1)^2 - q^2(g+f_v)^2 = 0$ $e_1 = \sqrt{1 - \exp(-2\lvert S\rvert)}$ $\left(\frac{1-e_1^2}{1-e_2^2}\right)^{n^*} = f_v\left(\frac{e_1}{e_2}\right)^3$ $with\ n^* = \begin{cases} 1, for\ prolate\ shape : 'p' \\ 1/2, for\ oblate\ shape : 'o' \end{cases}$	Considering the influence of pore shape, a model was used to describe the materials' dynamic behavior and constitutive relationship.

The integration of finite element subroutines and theoretical models for micropores growth, operating under specific assumptions about material properties, has spurred extensive research on the influence of stress triaxiality [53,125,126], porosity [127], size effects [102], crystal orientation [96,128,129], and temperature [130]. Among these factors, stress triaxiality has been identified as the predominant driving factor governing micropore growth and coalescence [89], which is highly similar to micropore nucleation. The growth of micropores is characterized as a function of the stress state, revealing significant variations in the evolution and shape changes of micropores under different stress triaxiality. Substantial alterations in micropore volume within materials occur at high-stress triaxiality, and material failure is primarily ascribed to the "porosity" effect. Conversely, under low-stress triaxiality, the shape changes in the micropores become more pronounced, and material failure is typically attributed to the "necking" of the micropores [131].

Table 2. Parameters in Table 1.

Model	Parameter	Meaning
Gurson model	σ_{eq}	The macroscopic von Mises equivalent stress.
	σ_0	The tensile yield stress of the ideal plastic matrix material.
	f_{v0}, f_v	Pore volume fraction.
	Σ_h	The macroscopic hydrostatic stress.
	ω, Ω	A porous representative volume element Ω containing pores that occupy volume ω.
	V_0, V	The initial and current volumes of the cell.
	E	Young's modulus.
GTN model	q_1, q_2, q_3	Calibration parameters.
	f_v^*	Functions related to f_v.
	σ_e	The flow effective stress of the matrix material.
		For most engineering alloys, f_{vC} is approximately 0.15.
		The pore volume fraction at the fracture.
	f_{vC}, f_{vF}, f_{vU}	The pore volume fraction at the ultimate value of the pore volume fraction.
LPD model	R, r	The initial and current radial distances of the RVE point from a fixed origin, respectively.
		Result from a re-calculation of the homogenization problem for hardening material.
	σ_{e1}, σ_{e2}	
GLD model	S	Aspect ratio.
	e_1, e_2	Parameters related to f_v and S.
	$C^*, \Sigma_z, \Sigma_r, \Sigma_h, \eta, q, g$	Parameters that can be exported from σ_{e1} and σ_{e2}.

Porosity describes the influence of the quantity and size of micropores on material performance. Higher porosity leads to poorer structural continuity and inferior material performance. In subsequent studies, numerous researchers have explored the impact of micropore size on material performance. Shu investigated the size effect of micropores under minor strain conditions using the elastic–viscoplastic strain gradient crystal plasticity theory [132]. Similar studies by Fang et al. [133] and Zeng et al. [134] have also employed the strain gradient crystal plasticity theory to explore the impact of micropore size on micropore growth. Their research consistently indicates that the growth of micropores exhibits a strong size effect, with smaller micropores often showing lower growth rates. Early research based on the Gurson criterion yielded results opposite to those of the studies mentioned above, suggesting that the growth of the micropores is independent of their size. However, with further research, the existence of size effects in ductile metallic materials has become undisputed.

Due to the limitations of macroscopic continuum models in understanding the microphysical mechanisms of the aforementioned micropore evolution, researchers have explored the stress variation trends around micropores at the mesoscale. Wang et al. investigated the interaction between micropore size and dislocations based on DD, finding that the critical stress required for dislocation emission depended on the size of the micropore. There was a decrease in the critical stress required for dislocation emission as the micropore size increased, thus affecting micropore growth [135]. The dislocation migration rate around micropores significantly influences micropore growth [136]. Small micropores have fewer dislocation sources, while large micropores have more, resulting in the faster growth of larger micropores. A DD simulation by Chang et al. further validated these findings [102], as shown in the corresponding simulation data in Figure 7.

With the development of single-crystal materials, the effect of crystal orientation on the growth of micropores is another area of research that has attracted widespread attention. This research aims to provide a unified explanation for the growth of micropores in single-crystal materials. Deng et al. [137], Murdoch et al. [138], Liu et al. [139] and Zhu et al. [140] conducted research on various materials under different conditions and

concluded that crystal orientation significantly influences the growth of micropores. Their research indicated that, under the same stress conditions, the shape changes in micropores and different loading directions can alter the orientation of the long axis of the micropore. Furthermore, the influence of crystal orientation on micropore growth is not uniform, with stress triaxiality and crystal orientation having competing effects on micropore growth [141]. Under low-stress triaxiality, the deformation mode mainly depends on crystal orientation. However, under high-stress triaxiality conditions, the rate of micropore growth is primarily determined by stress triaxiality and the initial pore volume fraction. Especially for smaller initial pore volume fractions, the growth rate of micropores is higher, emphasizing the significant influence of the initial crystal orientation.

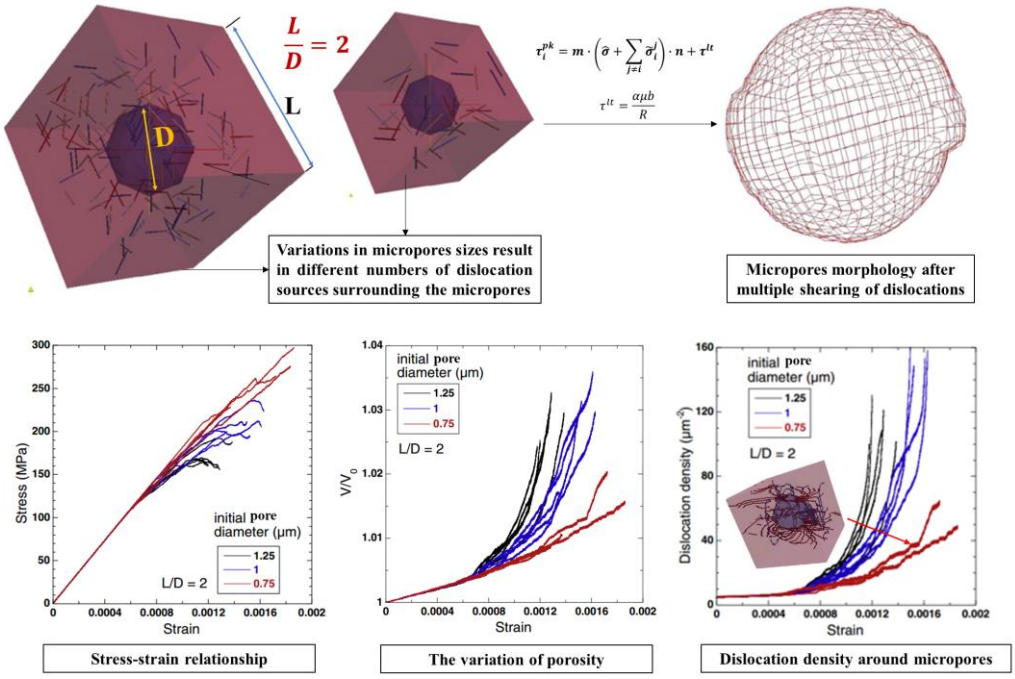

Figure 7. Influence of size effect on stress, dislocation density, and porosity change [102]. Reprinted with permission from ref. [102]; 2015 Scripta Materialia.

At a deeper microscale level, MD simulations have provided physical mechanisms for a significant amount of research [46,47,142]. Specifically, it has been observed that the tensile strength of the model increases as the ratio of micropore radius to system size decreases. This phenomenon is attributed to the scale-dependent stress required for micropore growth, which decreases with decreasing pore size. Consequently, the availability of the optimal shear surface decreases while the stress needed for initiating shear band nucleation increases. This is consistent with the experimental results of size effects in finite element simulations [143].

Our research group has conducted extensive MD simulations of micropore growth, investigating the effects of typical crystal orientations on the initial stress distribution, dislocation nucleation and emission, dislocation morphology, and stress–strain response in a nickel-based single-crystal matrix [144–146]. For instance, in one of our research projects [146], a size system 64.416 × 27.0336 × 5.28 nm^3 was chosen to investigate the orientation effect. Considering that the size of the model must be a multiple of the lattice spacing, the lattice spacing in the [109] oriented z is different from that of [99,108]. Periodic boundary conditions (PBCs) were applied to the z direction, and x and y were the shrink-wrapped boundary. A reasonable simulation of fracture and damage can be obtained considering that the potential energy can describe the bonding capacity in a metal system and the dependence of the strength of a single bond on the local environment (e.g., surface and defects) well. In addition, this EAM potential, based on the first principles, can

reproduce many fundamental properties, such as vacancy migration energy and unstable and stable stacking fault energy. Therefore, the embedded atom method of Ni developed by Mishin et al. [147] was used to simulate the uniaxial tensile behavior of single-crystal nickel with nanopores. A microcanonical ensemble was taken during the simulation process, and the temperature of the thermostat atom was controlled by rescaling the atomic velocity by 40 picoseconds in 1 fs time step. Finally, the open visualization tool (Ovito) of Stukowski [148] was used to observe and analyze the atomic configuration throughout the stretching process. The model's dimensions, boundary conditions, and simulation results are shown in Figure 8.

Based on the research achievements in crystal orientation, our research group has systematically summarized the impact of orientation deviation on the creep performance of nickel-based single-crystal superalloys [149]. Orientation deviation represents an essential form of crystal orientation affecting material performance, which arises due to the difficulty in precisely controlling temperature gradients and directions during the material solidification process. High-temperature creep experiments were conducted at two typical operating temperatures to evaluate the influence of orientation deviation. In addition, a constitutive model considering orientation deviation was proposed using the CPFEM finite element simulation method. The experimental results demonstrate that the orientation deviation effect on nickel-based single crystals under high-temperature and low-stress conditions gradually diminishes with increasing temperature. The specific experimental conditions and results are illustrated in Figure 9.

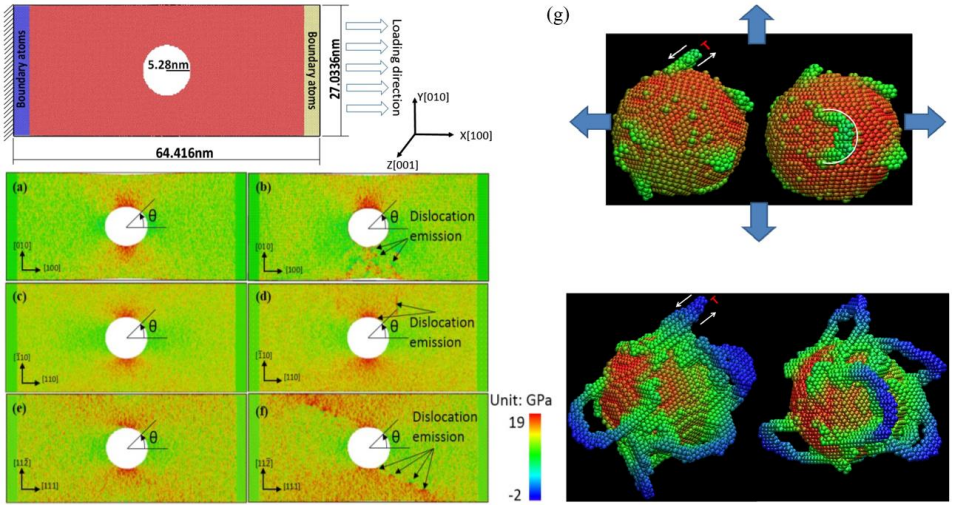

Figure 8. Contour maps of tensile stress fields of micropores with different orientations [146] (**a**) [99] orientation $\varepsilon = 0.045$ $t = 80$ ps; (**b**) [99] orientation $\varepsilon = 0.05$ $t = 100$ ps; (**c**) [108] orientation $\varepsilon = 0.032$ $t = 41$ ps; (**d**) [108] orientation $\varepsilon = 0.034$ $t = 64$ ps; (**e**) [109] orientation $\varepsilon = 0.030$ $t = 56$ ps; (**f**) [109] orientation $\varepsilon = 0.031$ $t = 60$ ps; (θ is a horizontal angle); (**g**) Shear ring formation and expansion side and top views [150]. Reprinted with permission from ref. [146,150]; 2017 Computational Materials Science, 2012 Acta Materialia.

For polycrystalline materials, the crystal orientation of the polycrystal is random, and due to the influence of crystal orientation and grain geometry, sometimes tiny pores grow faster than larger micropores [151]. In addition, MD simulations are more often used to elucidate the micropore growth mechanism [104,135,152–154]. Previous studies on the physical mechanisms of micropore growth have proposed two main mechanisms that influence this process: vacancy condensation and dislocation release [153,155,156]. The applicability of these theories depends on factors such as temperature, strain rate, and the localization of plastic flow. Under low-temperature and high-strain-rate conditions, the primary mechanism of micropore growth is dislocation emission triggered by high-stress concentrations. Prism and shear dislocation loops are carriers for atomic transfer radially

from the pore front. As the dislocation loop propagates from the pore front, existing micropores grow, leading to the eventual coalescence of initially separated micropores. This coalescence further enhances micropore growth.

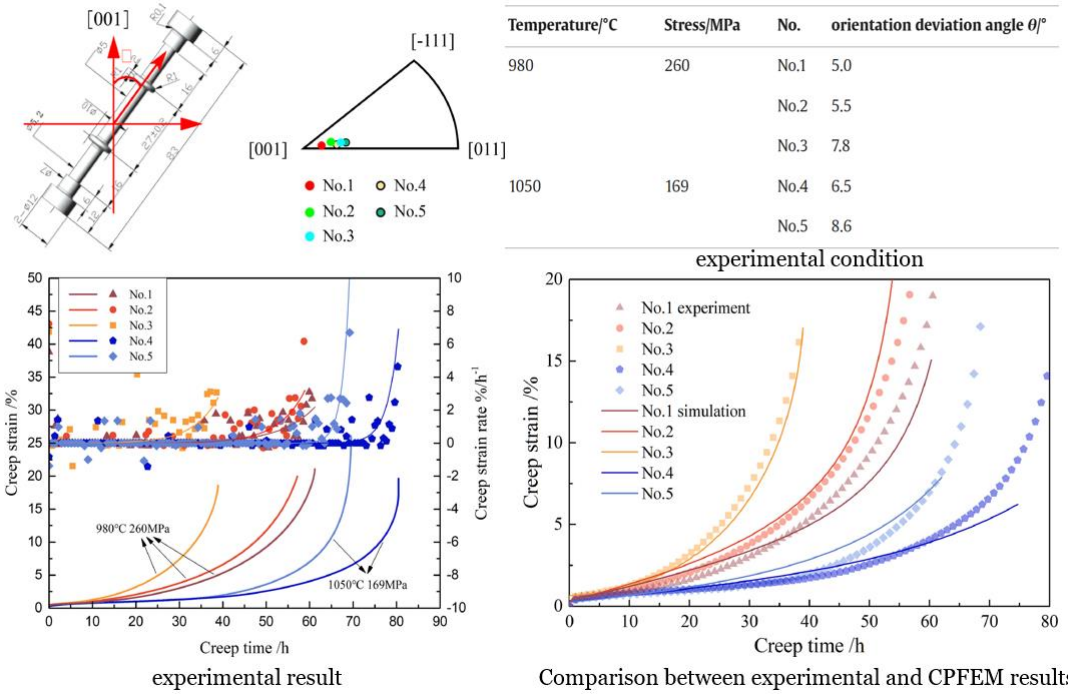

Temperature/°C	Stress/MPa	No.	orientation deviation angle θ/°
980	260	No.1	5.0
		No.2	5.5
		No.3	7.8
1050	169	No.4	6.5
		No.5	8.6

Figure 9. The effect of orientation deviation on the creep properties of nickel-based single-crystal high-temperature alloys [149]. Reprinted with permission from ref. [149]; 2023 International Journal of Plasticity.

Davila [157] proposed the theory of prism loops and shear loops (as shown in Figure 10) to describe the microscale mechanism of internal micropore growth in various materials. Before this, prism loops were already well-known among researchers, with studies by Seppälä et al. demonstrating that prism loops are the primary form of micropore growth, achieved through the emission of dislocation loops [158]. The concept of shear loops is relatively novel. However, the emission of shear dislocation loops from the surface of micropores, similar to Ashby's geometrically necessary dislocations, is consistent with experimental observations. Therefore, there is considerable controversy regarding the microscale growth mechanisms for prism loops and shear loops in micropores. Meyers et al. conducted a series of studies and confirmed, through relevant uniaxial tension simulation results, that shear dislocation loops are the primary mechanism for micropore growth. Their simulation results noted no prism dislocation loops [53,126,159–161]. Tang et al. found that the emission of dislocation loops is the primary cause of micropore growth, and that the continuous nucleation of dislocations and the increase in shear loops promote micropore growth [54].

Research on the micropore growth mechanism has made relevant progress. However, a comprehensive and universally applicable description has yet to be obtained. Therefore, it is necessary to establish micropore growth theories and models at the micron and nanoscale levels, considering additional influencing factors, including 3D morphology, spatial distribution characteristics, stress states, and external environment. By incorporating these factors into the model, a more complete understanding of micropore growth can be obtained.

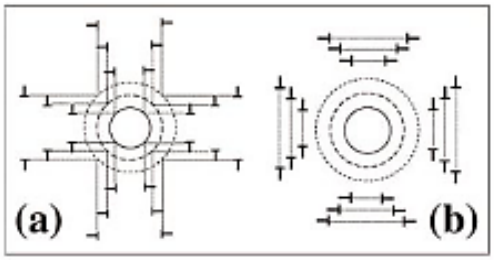

Figure 10. Microscopic mechanism of micropore growth [157]: (**a**) shear ring; (**b**) prismatic ring. Reprinted with permission from ref. [157]; 2005 Applied Physics Letters.

The multiscale model formed by CPFEM, DD, and MD coupling comprehensively describes the performance and behavior of materials from the macroscopic scale to the atomic level. In the study of pore growth mentioned above, the advantage of CPFEM lies in the simulation, while its role in studying the fundamental physical mechanisms at small scales is limited. In contrast, MD is suitable for describing the atomic-scale behavior of materials, simulating atomic interactions and the microstructure of materials, and exploring the fundamental physical laws that control material behavior. Many studies [65,162–164] have utilized multiscale models to analyze materials comprehensively. This type of multiscale model can more accurately predict the mechanical properties, damage behavior, and deformation mechanisms of materials, providing a deeper understanding and support for material design and engineering applications.

4. Collapse

The growth and collapse of micropores in ductile metallic materials are fundamental processes that ultimately lead to material failure under tensile and compressive loads [165]. In other words, the growth or collapse of micropores in materials is a consequence of deformation under varying stress conditions. Factors like crystal orientation and other intrinsic material properties likely exhibit considerable similarity in their impact on micropore behavior. Nevertheless, additional research is necessary to investigate whether these influencing factors and stress conditions compete or interact synergistically. Due to the similarities among these influencing factors, numerous scholars have directed their efforts toward comprehending the connections and distinctions between micropore growth and collapse. In the study conducted by Liu et al. [166], the critical strain for micropore growth and collapse was investigated using homogenized micromechanics. They identified the load parameter and stress triaxiality associated with the crucial strain during micropore growth and collapse. Significantly, as depicted in Figure 11, it was observed that the stress state corresponding to the transition from pore growth to collapse is discontinuous, exhibiting a transitional zone in between. Within this transition region, the material experiences neither growth nor collapse.

While considerable attention has been dedicated to comprehending the response of materials to impact and compression, there has been relatively less investigation into the ductile failure stemming from micropore collapse. Theoretical examinations of the deformation behavior of individual micropores in power-law materials under uniform stress have unveiled that an initially spherical micropore can transform shape into an ellipsoid before collapsing structures resembling cracks or needles [167]. Detailing the mathematical formulation of pore collapse has been crucial in developing material constitutive equations for impact compression scenarios. However, research explicitly addressing shock-induced pore collapse remains relatively limited, with only theoretical models based on dislocation mechanisms proposing rapid sliding prismatic dislocation ring emission as the mechanism for micropore collapse. The models mentioned above were successfully applied to shock wave propagation in porous materials [168–171]. The introduction of one of the models is shown in Table 3, and the meanings of the parameters in Table 3 are shown in Table 4.

However, the physical processes leading to micropore collapse remain unresolved, and the underlying mechanisms remain poorly understood.

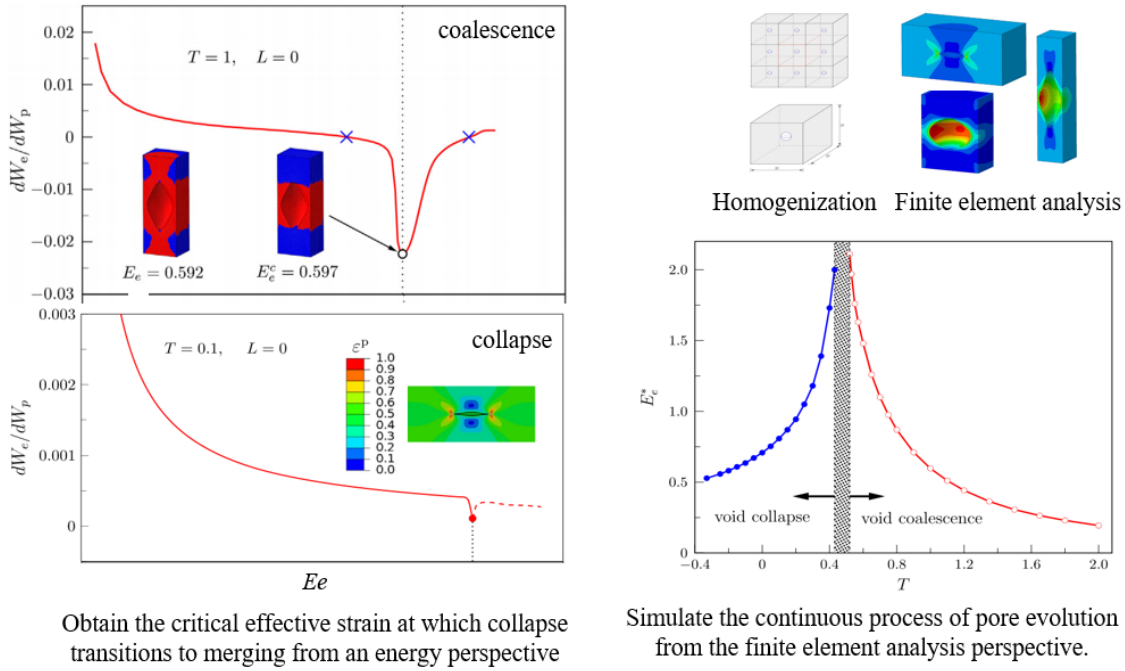

Figure 11. Relationship between critical macroscopic effective strain and stress triaxiality (transition region between pore collapse and pore coalescence is represented by shadow) [166]. Reprinted with permission from ref. [166]; 2016 International Journal of Plasticity.

MD simulation has been extensively employed since 2000 to investigate its microscopic atomic mechanism and comprehensively understand micropore collapse. Through MD simulations, Solanki et al. [172] explored cylindrical pores' partial and complete collapse behavior in high-strain-rate monocrystalline copper and nickel. They compared the results with finite element analysis and experimental data, particularly regarding local inelastic flow. Interestingly, despite the substantial spatiotemporal scale difference between the methods, the results exhibited high consistency. Non-equilibrium molecular dynamics (NEMD) calculations conducted by Davila [157] demonstrated that impact-induced micropore collapse in copper occurs through the emission of shear rings, differing from the prismatic rings assumed by conventional continuum mechanics models. Liao et al. systematically investigated the collapse of micropores in np-Ni with graded micropores under NEMD. Their findings reveal that the collapse rate of micropores is linearly dependent on the impact loading speed. Furthermore, the initial surface dislocation location of micropore collapse is influenced by the position of the micropores in the sample and the size gradient of the micropores [171]. Prasad et al. Investigated the micropore collapse mechanism of nickel single crystals using atomic simulation methods and explored the impact of temperature micropore collapse [173]. Their results revealed that the emission and interaction of dislocation rings around micropores were the primary mechanisms of micropore collapse, and the rate of micropore collapse was almost temperature-insensitive. Furthermore, more and more studies have suggested that the shear ring mechanism of micropore growth also plays a significant role in micropore collapse and is one of the primary mechanisms involved. Guan et al. investigated the collapse behavior and mechanism of micropores in single-crystal aluminum through 1D and 3D MD compression simulations. The results of the simulations demonstrated that dislocation shear rings, as depicted in Figure 12, were emitted from the surface of micropores during both 1D and 3D compression. The distinction was that, in 3D, dislocation shear rings converged to form two intersecting tetrahedrons, thereby reducing the collapse rate of the micropores [174].

Table 3. A pore growth/collapse model based on iterative methods.

Model	Equation	Description
Basic equations	$Q = \mathrm{e_n} \otimes \hat{e}_n$	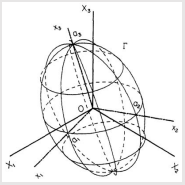 By iterating the method, the pore model gradually approximates the complex deformation of the actual pore.
Equilibrium equation	$\sigma_{ij,j} = 0$	Neglecting the inertia term and ignoring the pore rotation caused by elastic deformation.
Equation of motion relationship	$u_{i,j} = (d_{ij}^{(e)} + w_{ij}^{(e)}) + (d_{ij}^{(p)} + w_{ij}^{(p)})$ $d_{ij}^{(p)} = p_{ij}^{\alpha}\dot{\gamma}^{\alpha}, w_{ij}^{(p)} = \omega_{ij}^{\alpha}\dot{\gamma}^{\alpha}$ $p_{ij}^{\alpha} = \frac{1}{2}(s_i^{\alpha}n_j^{\alpha} + s_j^{\alpha}n_i^{\alpha})$ $w_{ij}^{\alpha} = \frac{1}{2}(s_i^{\alpha}n_j^{\alpha} - s_j^{\alpha}n_i^{\alpha})$	The velocity gradient is decomposed into elastic and plastic contributions to make the motion equation more accurate.
Constitutive equation	$\dot{\sigma}_{ij} = L_{ijkl}d_{kl}^{(e)}$ $Li_{jkl} = \lambda\delta_{ij}\delta_{kl} + \mu\delta_{ij}\delta_{kl} + \mu\delta_{il}\delta_{jl}$ $\dot{\gamma} = \eta(\tau/\tau_n)^n$	The constitutive relations are simplified by the assumption that the contribution due to the rotation of the frame, caused by elastic lattice distortion, is negligible.

Table 4. Parameters in Table 3.

Model	Parameter	Meaning
Basic equations	X_n, x_n	Two coordinate systems. X_n are fixed and x_n rotating along the central axis of the pore.
	$\hat{e}_n, e_n$	The orthonormal triads in X_n and x_n coordinate system.
	Q	The rotation tensor, which transforms e_n into $\hat{e}_n$.
Equilibrium equation	$\sigma_{ij,j}$	The Cauchy stress.
Equation of motion relationship	$v_{i,j}$	The velocity vector.
	$d, w; e, p$	d and w are the deformation rate tensor and the spin tensor, respectively, and the superscript e stands for the elastic part, while the superscript p stands for the plastic part.
	$\alpha\dot{\gamma}^{\alpha}$	α is summed over all active slip systems and $\dot{\gamma}^{\alpha}$ is the slip rate of the α slip system.
	s^{α}, n^{α}	s^{α} and n^{α} are the tangential and normal unit vectors of the α slip system, respectively.
Constitutive equation	L	L is the fourth-order elasticity tensor.
	λ, μ	λ and μ are the Lame constants, $\delta_{i,j}$ is the Kronecker delta.
	η, τ_r, n, τ	η and τ_r are n regarded as material parameters, and τ is the resolved shear stress component in the slip direction.

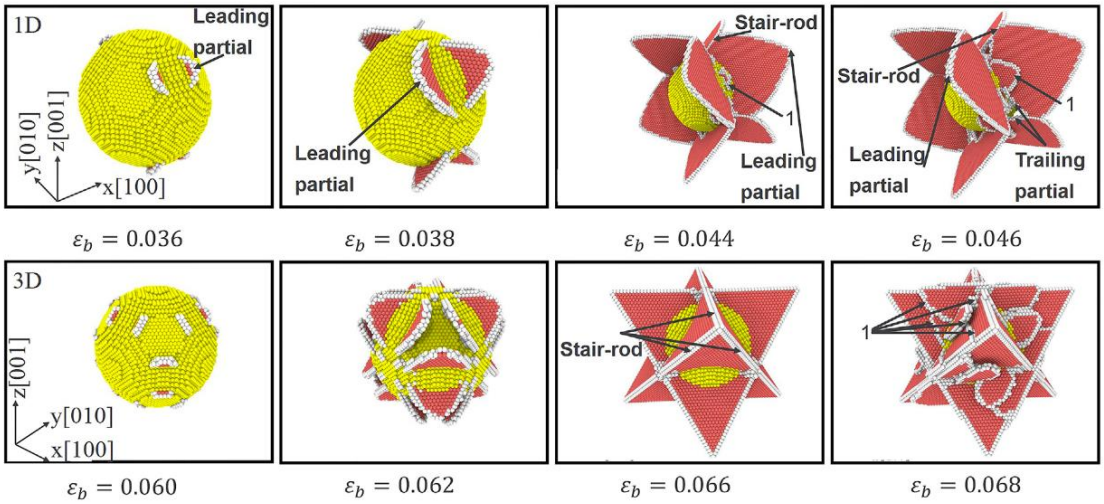

Figure 12. Dislocation emission and growth with a visible dislocation shear ring on a micropore's surface during the micropore's collapse [174]. Reprinted with permission from ref. [174]; 2019 Computational Materials Science.

In addition to face-centered cubic metals, as mentioned above, relevant studies have also explored the collapse behavior of micropores in body-centered cubic and close-packed hexagonal metals [175,176]. Furthermore, additional factors, such as temperature and hydrostatic pressure, have been considered [173,177,178]. Vacancy diffusion contributes to dislocation movement at higher temperatures and promotes continuous micropore collapse. At lower temperatures, the collapse behavior of micropores in body-centered cubic and close-packed hexagonal metals has been improved. Mass transport and micropore collapse occur through dislocation formation, slip, and interaction, resulting in strain hardening. Due to the strain hardening around micropores at lower temperatures, compared to higher temperatures, the collapse of micropores is delayed after the initial stage of closure, further enhancing the understanding of micropore collapse. However, a substantial gap exists in the research on micropore collapse compared with micropore growth. More complex factors must be considered, and the synergistic and competitive effects between different factors must be discussed in detail. Moreover, current simulation studies on micropore collapse mainly focus on high-impact rates, and the influence mechanism under the low-speed action has not been thoroughly studied and understood.

5. Interference between Micropores

When micropores reach a certain extent of growth or collapse, they coalesce with neighboring micropores. However, the interaction between micropores is often overlooked in the later stages of growth and deformation, as well as before coalescence. An interactive relationship exists between micropores even before they physically come into contact, as shown in Figure 13. Currently, a mutual disturbance between micropores has been observed in experimental phenomena. This interaction between micropores can also be referred to as micropore interference.

Tvergaard and Niordson studied the interaction between large and small pores. They found that the growth of tiny pores was significantly limited by the stress concentration effect of nearby large pores when their size length was comparable to the material's characteristic length scale [179]. Furthermore, other researchers have investigated the influence of initial pore spacing on the evolution of two pores before coalescence [131,180–182]. For instance, Cui et al. studied the interaction between two elliptical pores under uniaxial loading. By controlling the direction of the long axis of the elliptical pores and the ratio of their long axis length ($2a_1$) to short axis length ($2a_2$), three shape combinations, as shown in Figure 14, were formed. Their study also discussed the influence of the initial pore spacing (ILD0) Different shape combinations will affect the number of dislocation emissions around

the micropores, especially when the micropore spacing is small. The micropores' shape combination determines whether dislocation emission is promoted or suppressed. The starting point of multi-elliptic micropores cluster dislocation emission mainly depends on the micropores whose central axis is perpendicular to the uniaxial loading direction [180].

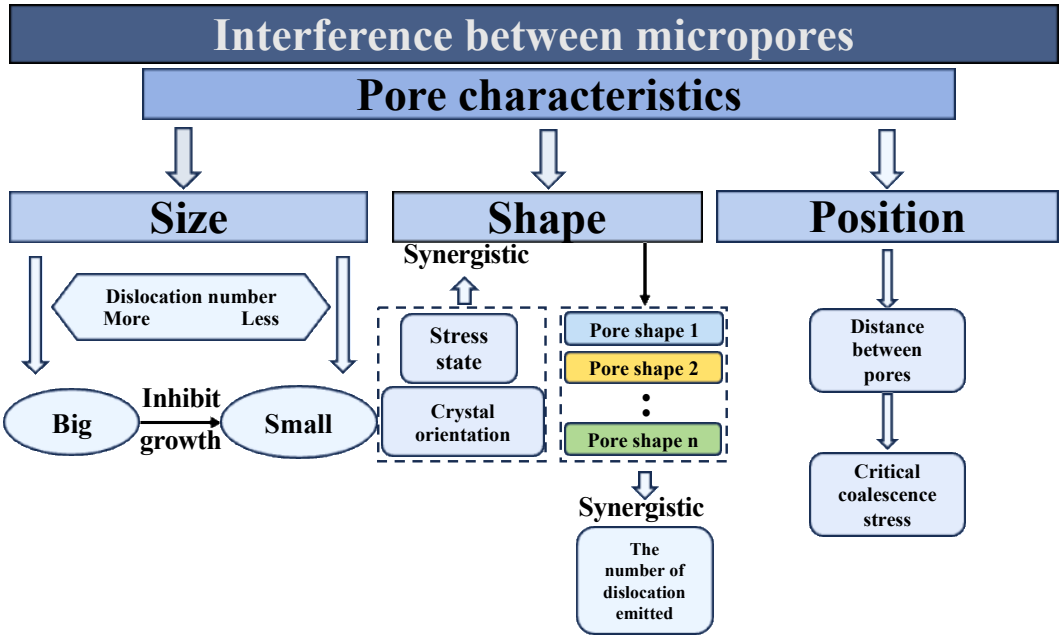

Figure 13. Summary of micropore interaction.

The two-pore system exhibits a higher likelihood of yield than the single-pore system, with a more minor critical yield stress [183]. This behavior can be attributed to local elastic and plastic deformation fields forming around each micropore. Each micropore generates a local elastic strain field, typically associated with the expansion center, which expands their interaction range. For instance, the shear stress decreases as the distance from the micropores increases, and when micropores are sufficiently close, the neighboring pore's stress field can alter each micropore's growth rate. The changes in the elastic field affect the activation of plastic deformation and subsequent expansion of the plastic zone surrounding the micropores. Micropores can also interact through their plastic fields, which may increase local hardening rates, heat softening, and shear localization.

The concept of a transition to shear deformation, proposed by Brown and Embury based on simple geometric considerations, suggests that the critical inter-pore ligament distance should be equal to the diameter of a micropore [184]. In other words, when the surfaces of a pair of micropores are separated by a distance equivalent to a single micropore's diameter, they transition from independent growth to interaction. According to this idea, it is at this point that the dominant micropore process changes from radial plastic flow around isolated growing micropores to shear deformation, facilitating the rapid coalescence of micropore pairs. However, recent studies have indicated that the micropore growth rate increases for distances between micropores up to six times the diameter [185–187]. This necessitates additional research on microscopic mechanisms. E. T. Seppälä conducted extensive studies using 3D MD simulations to investigate micropore interactions. This included quantifying the reduction in distance between micropores, directional growth of micropores, and corresponding shape evolution. In agreement with Brown and Embury's thesis, the growth rate of micropores was examined, revealing that the interaction between micropores is not reflected in the volume growth rate [158].

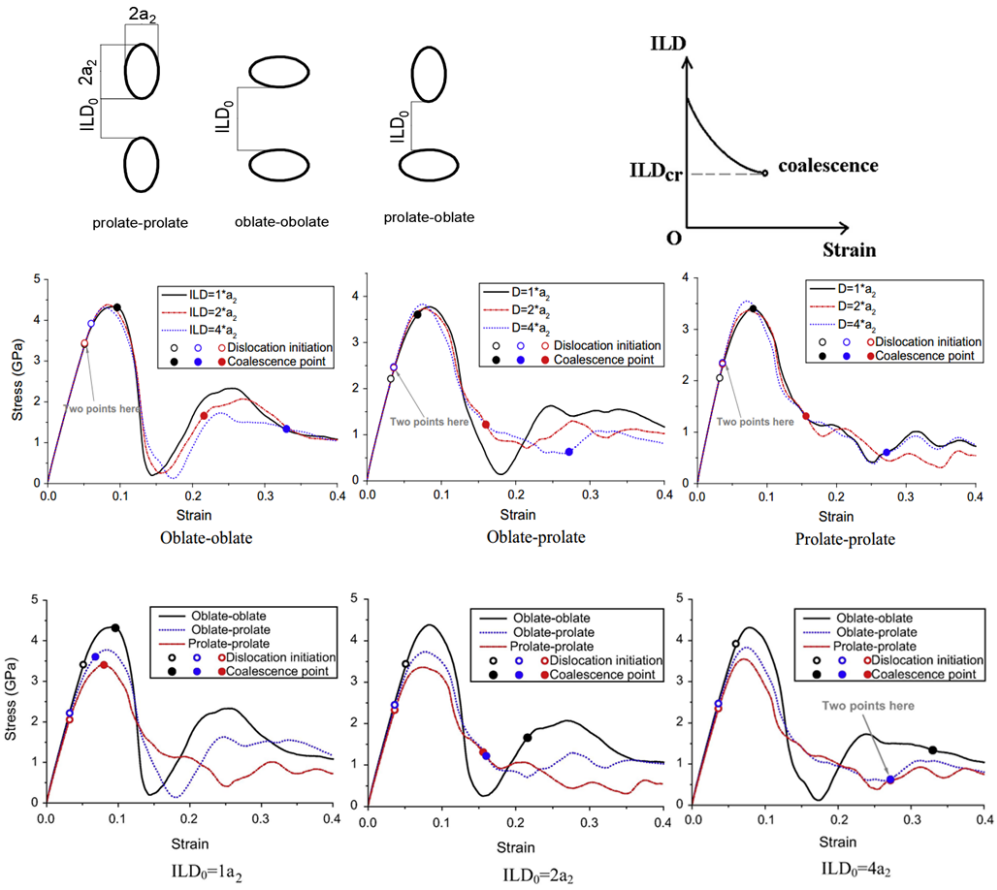

Figure 14. The influence of the shape combination and ILD0 of micropores on material properties [180]. Strain–stress curves to reflect the influence of ILD0; Strain–stress curves to reflect the influence of pore shape combination. Reprinted with permission from ref. [180]; 2015 Computational Materials Science.

Numerous macro and micro studies have demonstrated that interpore interference originates from the slip zone [91]. In prior research [91,104,106,110,112,113,152,188,189], the authors conducted MD simulations on multiple micropores with varying configurations to examine the evolution of micropores from the elastic to the plastic stage. They compared the effects of micropore evolution and interaction on fundamental mechanical properties under different configurations and analyzed the alterations in stress distribution and stress triaxiality throughout the evolution process. The additional analysis involved studying dislocation nucleation, dislocation density, and stacking fault trends to understand the different forms of micropore interactions. Two distinct interference mechanisms were identified: (1) local plastic deformation and (2) uniform plastic deformation.

Furthermore, local plastic deformation was subdivided into local necking and local shear, enabling an assessment of the mechanisms behind micropore interference and plastic deformation. The distinction between these two deformation mechanisms is primarily attributed to the competition and synergy between stacking faults and dislocation density. Stacking faults predominantly influence local plastic deformation, whereas uniform plastic deformation is mainly governed by dislocation motion, with minimal occurrences of stacking shear motion, as shown in Figure 15.

The dynamic evolution and deformation behavior of micropores and the interactions between multiple micropores are highly complex, involving intricate physical and mechanical processes, including stress transfer, concentration, and strength degradation. Due to the complexity of micropore evolution and the current limitations in microscale pore characterization, most studies on pore–pore interactions still rely on simplified models to investigate interactions between pores, such as geometric arrangements, pore shapes, and

distances between pores. At the same time, some factors involving complex influencing mechanisms may be overlooked.

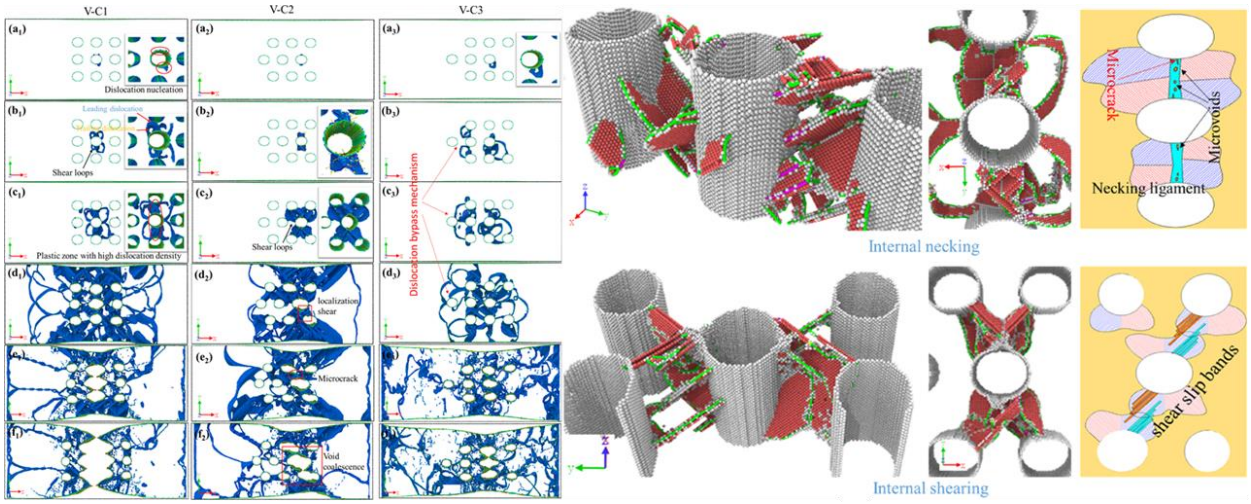

Figure 15. Local plastic deformation of microstructure evolution at different strain: (**a1**) ε = 0.05925, (**b1**) ε = 0.0613, (**c1**) ε = 0.06332, (**d1**) ε = 0.08013, (**e1**) ε = 0.1423, (**f1**) ε = 0.23769; Microstructure snapshots of configuration2 at different strain: (**a2**) ε = 0.04866, (**b2**) ε = 0.05276, (**c2**) ε = 0.05687, (**d2**) ε = 0.07553, (**e2**) ε = 0.08611, (**f2**) ε = 0.14415; Microstructure snapshots of configuration3 at different strain: (**a3**) ε = 0.05279, (**b3**) ε = 0.05689, (**c3**) ε = 0.05892, (**d3**) ε = 0.06515, (**e3**) ε = 0.18652, (**f3**) ε = 0.2373, and micropore interaction [190]. Reprinted with permission from ref. [190]; 2019 Journal of Applied Physics.

In the future, it is necessary to develop advanced experimental techniques and numerical models to delve deeper into the quantitative characterization of inter-particle interactions. The ultimate goal is to understand the underlying mechanisms governing these interactions comprehensively. In addition to simple inter-pore interactions, future research should consider the influence of other microstructural features, such as grain boundaries, inclusions, and precipitates. Furthermore, investigations should encompass different material systems and loading scenarios to comprehensively understand how these interactions vary under diverse material compositions and loading conditions. The aim is to achieve a comprehensive understanding of the interaction mechanisms.

6. Coalescence

The coalescence of micropores is a crucial damage mechanism that significantly impacts material deformation [141,191]. Diverse methodologies have been employed to investigate micropores coalescence. Some crucial models related to pore coalescence are also proposed. For example, McClintock's model [192], the model of Hancock and McKenzie [193], the model of Budiansky, Hutchinson, and Slutsky [194], and Thomason's model [195–198]. Thomason [197] proposed a method in 1985 to locate the onset of pore coalescence. Subsequently, Benzerga and Leblond [199] revisited Thomason's work and derived a fully analytical solution for pore coalescence by considering circular cylindrical geometric shapes and velocity fields suitable for constrained plastic flow configurations.

Presently, the computation and exploration of micropore coalescence primarily consider factors such as crystal orientation, stress triaxiality, spatial configuration of the micropores, micropore spacing, shape, and strain hardening coefficient [200–202]. Certain studies simulate the coalescence behavior by considering adjacent micropores' spatial configuration or the size/spacing ratio [203]. Others investigate the plastic loading limit deformation of non-hardened materials containing regular arrays of micropores [96,139,204]. In subsequent studies, Pardoen and Tekoglu classified micropores' coalescence into stretch coalescence or shear coalescence based on the ligament orientation between the two coalesc-

ing micropores [205,206]. Liu et al. explored the coalescence behavior of single-crystal micropores, grain boundary micropores, and two-grain micropores employing a twin-crystal model [207]. Under strain-controlled boundary conditions, micropores in soft-oriented grains demonstrated a greater inclination to coalesce than those in hard-oriented grains. In the coalescence of grain boundary micropores, the deformation mismatch between grains is heightened with the difference in orientation factor, fostering micropores' growth along the grain boundary. A notable distinction in orientation factors expedited the coalescence of micropores at grain boundaries while decelerating the coalescence of micropores within grains. Any micropore coalescence model must integrate microstructural details, including micropore/ligament length and geometry. Deng et al. employed MD simulations to explore the impact of micropore configuration on the coalescence of single-crystal copper micropores under impact loading [137]. During the tension stage, the micropores initially grew independently, followed by a coalescence process resembling the nucleation of micropores observed in the spallation of simulated single-crystal copper [204]. Numerous small micropores formed along the spatial ligaments of the two micropores and rapidly coalesced to create a channel wherein the two micropores merged. However, the coalescence rate of micropores varied with different loading angles, with a higher likelihood of micropore coalescence occurring when the impact direction was connected to the center of the two micropores at a 60° angle.

Interference between micropores has been identified through experimental observations. Various mechanisms related to micropore coalescence have been summarized [103,111,208–213]: The primary and most prevalent mechanism entails coalescence through the internal neck constriction of the inter-micropores' ligament, with the critical ligament distance parameter determining the coalescence point (Figure 16a). The second type involves connection through narrow shear plates, a phenomenon frequently observed during shear-induced micropore deformation (Figure 16b). A third, less common mechanism is referred to as columnar coalescence or neck condensation, wherein micropores coalesce along their length (Figure 16c). This situation is encountered in steels with elongated inclusions [214] or alloys with arranged clusters of particles [215]. Figure 16d presents an example of the first mechanism of micropore coalescence, while Figure 16e illustrates an example of the second coalescence mechanism.

By replicating the structural evolution at the atomic scale, involving dislocation motion and atomic diffusion [143,216], MD simulations of micropore coalescence can offer insights into evolution mechanisms inaccessible in larger-scale simulation studies. Seppälä, through MD studies, discovered that the coalescence process of isolated micropore pairs at the microscale significantly differs from the coalescence process of single micropores at periodic boundaries, emphasizing the limitations of the latter in describing coalescence in typical low-symmetry configurations [158]. Zhao et al. conducted MD simulations to investigate the growth and coalescence of two micropores in single-crystal copper, considering two influential factors: the initial radius and spatial distance between the micropores [182]. They observed that the peak stress triaxiality increased with the initial distance of the micropores ligament until reaching the critical coalescence point, after which it decreased. This suggests that stress triaxiality may be a significant indicator for determining micropores coalescence. Besides the coalescence mechanisms, the conditions under which micropore coalescence occurs have also received extensive attention. Le et al. described coalescence as happening when the long axis of a micropore is an order of magnitude of the average spacing between adjacent planes [209]. Koplik and Needleman determined the onset of micropores coalescence through single-cell analysis, identifying the transition to a uniaxial stretching state in the macroscopic deformation of the cell [111]. These findings emphasize the significance of micropore growth and coalescence in the plastic deformation of porous materials.

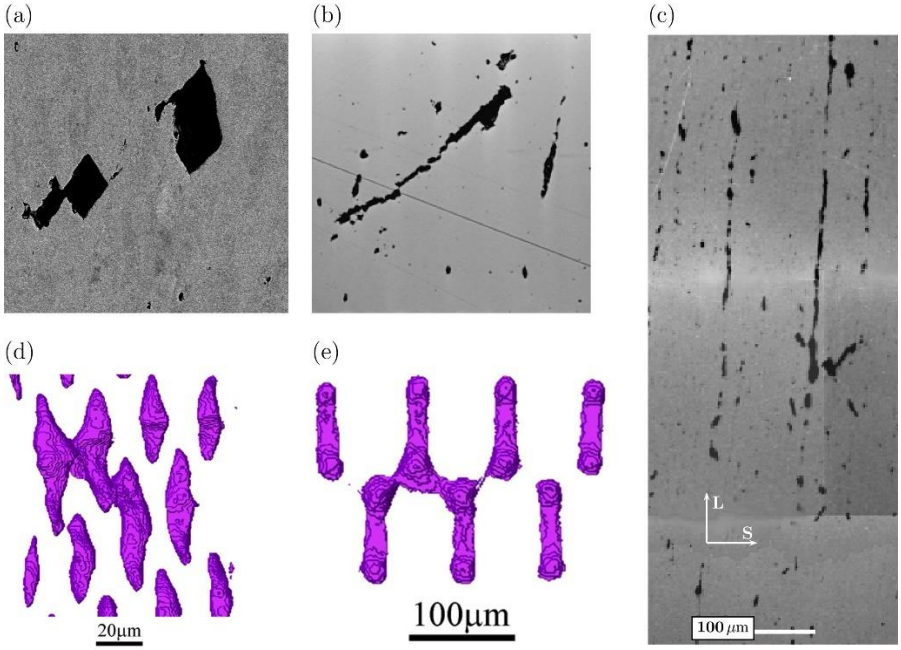

Figure 16. Mechanism and examples of micropore coalescence [217,218]. Reprinted with permission from ref. [217,218] (**a**) Coalescence occurs through the contraction of the inner neck of the microporous ligament; (**b**) Coalescence of micropores caused by shear; (**c**) Columnar coalescence; (**d**) Example of a coalescence mode; (**e**) Example of b coalescence mode; 2008 Acta Materialia, 2002 Modelling and Simulation in Materials Science and Engineering.

In addition to studying the evolution mechanism of micropores themselves, MD simulations are commonly used to explore the impact of micropore aggregation on the mechanical properties of materials, providing a theoretical basis for designing and controlling advanced materials. For instance, using MD simulations, Tran et al. investigated the deformation mechanism and mechanical properties of Cu-Ta metallic glass nanofilms containing one and two micropore defects during the tensile process [182]. They found that the tensile strength of the specimen with two micropores was higher than that of the specimen with one micropore, although the failure rate was faster. This phenomenon has been previously reported in studies conducted by Mi et al. [219]. The findings suggest that porous samples generally exhibit higher yield stress and greater load-bearing capacity than single micropore samples, primarily due to the enhanced dislocation interaction under constant porosity conditions. This observation indicates that sample stress resistance can be improved by redistributing a large micropore into multiple smaller micropores at the nanoscale. However, the evolution of the micropores' ratio appeared to be independent of the number of micropores, and no significant acceleration in the micropores' expansion resulting from the coalescence of adjacent micropores was observed. Gao et al. investigated the influence of micropores on the mechanical properties of FeNiCrCoCu high-entropy alloys [220]. They examined different micropore sizes, applied strain rates, and temperatures, analyzing the evolution behavior of micropores using a model with one or two micropores. The research team also conducted MD simulations to study the coalescence of micropores, explicitly discussing the coalescence evolution behavior of micropores in the matrix phase of nickel-based single-crystal alloys. The study explored the effects of crystal orientation and initial radius of micropores, obtaining mechanical property parameters such as stress-strain curves, as well as micro deformation mechanisms such as micro error evolution [183].

Additionally, it was observed that materials with two micropores were more malleable and deformable compared to those with only one micropore (Figure 17). In conclusion, micropore coalescence behavior, a crucial aspect of the fracture failure process in ductile

materials, has garnered increased attention, particularly in emerging materials and high-end manufacturing industries. In the later stages, it becomes imperative to consider the service performance of micro–nano processing and nanocrystalline materials. Indeed, the advancement in multi-scale calculation methods such as MD, DD, and CPFEM, along with complementary microscopic observation and characterization technologies, holds great promise. These developments contribute to micropore coalescence research and provide a solid theoretical and experimental foundation for performance design, control strategies, and the evaluation of performance and service life in materials at the atomic and microstructural levels.

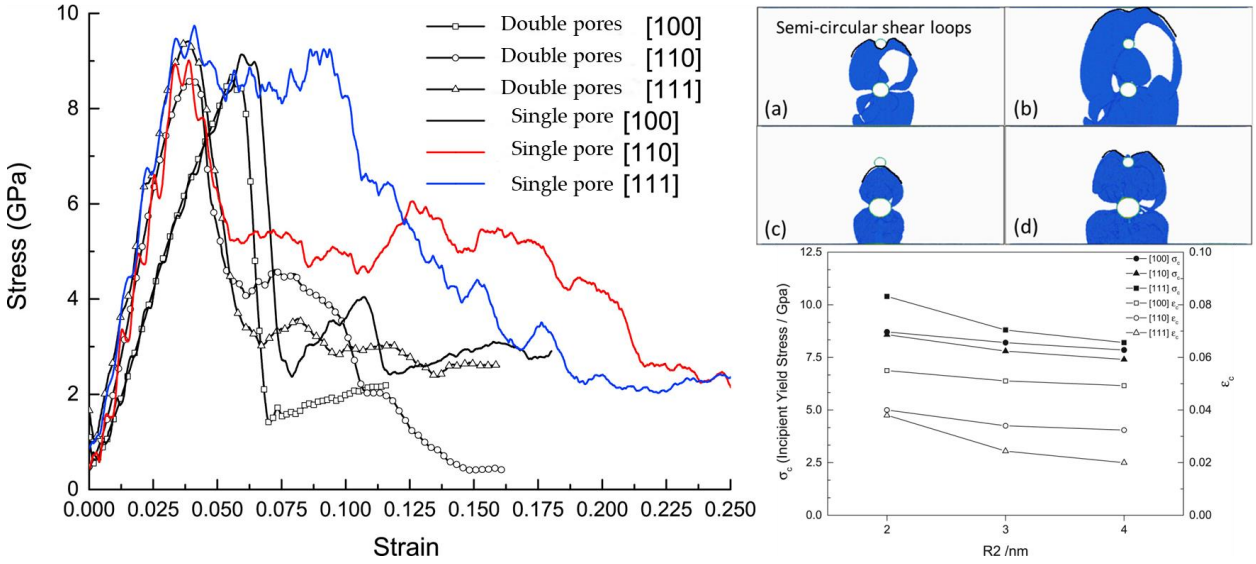

Figure 17. The influence of the number, size, and crystal orientation of micropores on materials [183]. (**left**) Comparison of stress–strain curves of single-pore and two-pore models; (**right**) variation trend of yield strain and yield stress under different orientations and different second micro pore radii: (**a**) R_2 = 3 nm, ε = 3.5%; (**b**) R_2 = 3 nm, ε = 3.7%; (**c**) R_2 = 4 nm, ε = 3.6%; (**d**) R_2 = 4 nm, ε = 3.7%. Reprinted with permission from ref. [183]; 2018 Current Applied Physics.

7. Interaction between Micropores and Other Microstructures

The predominant focus of studies on the growth and coalescence behavior of micropores has been on single-phase materials. However, the mechanical properties of most metal materials in their natural state are anisotropic. These materials exhibit diverse microstructures with varying properties, including different crystal orientations and phase interfaces, which significantly influence the evolution of micropores. In the case of polyphase or polycrystalline materials, the external environment surrounding micropores also impacts the material's mechanical properties. In particular, when micropores appear in phase interfaces, the load-bearing capacity of the material is significantly reduced.

Moreover, the deformation and growth of micropores differ due to variations in the structure and physical properties of different phases. Hence, it becomes imperative to study the influence of the local environment (i.e., the matrix material with different microstructures) on the deformation and growth behavior of micropores and the resulting mechanical properties of the material. Recently, there has been a growing emphasis on studying defects like micropores and exploring their interactions with different microstructures [221–224]. Figure 18 shows the synergistic effect between dislocation and micropore spacing on pore growth at the finite element scale. The small size of the micropores and microstructures makes it challenging to directly observe material deformation mechanisms using existing experimental testing methods, with only a few high-cost and high-resolution TEM in situ tests available. As a convenient method for observing atomic motion in real time and understanding the interaction mechanisms between micropores and various

microstructures, MD simulation has found widespread application in nuclear reactor materials [40,225,226], advanced high-temperature alloys [187,227], and other studies related to internal micropores and dislocations [228–230]. Moreover, it has been employed to investigate the interaction between precipitated phases, microcracks, and other internal micropores, considering changes in mechanical properties and radiation resistance [222].

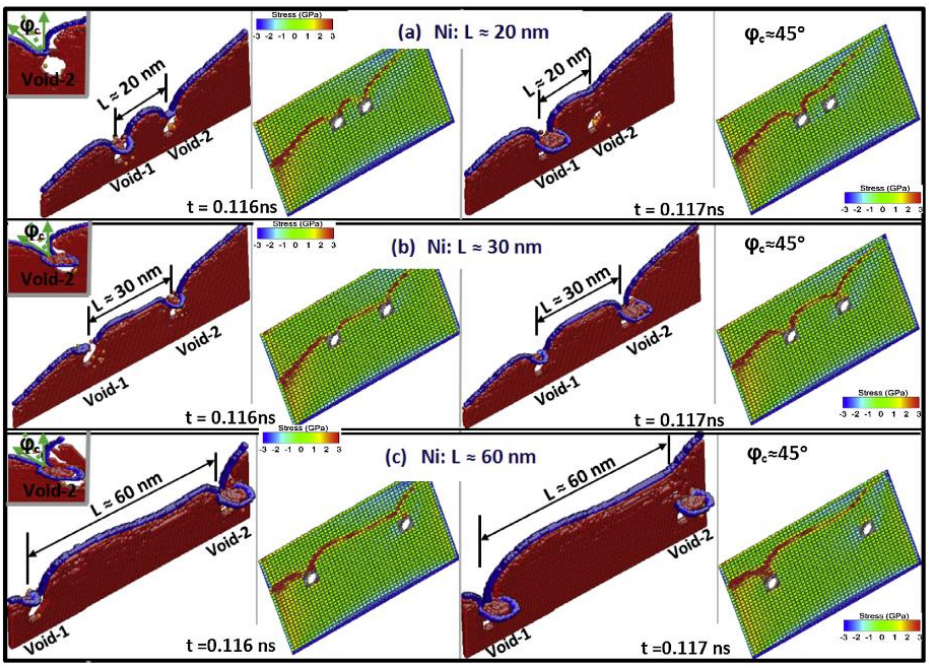

Figure 18. From [109]; Plane dislocation, stacking fault structure, and shear stress [230]. (**a**) L ≈ 20 nm; (**b**) L ≈ 30 nm; (**c**) L ≈ 60 nm. Reprinted with permission from ref. [230]; 2015 International Journal of Plasticity.

The interaction between micropores and other microstructures in a material is dictated by their sizes, shapes, and positions, consequently influencing the material's properties. The size of micropores, termed the size effect, is intricately linked with dislocation movement. Previous studies [136,231–233] have explored the interaction between micropores and dislocations in face-centered cubic crystals, utilizing MD simulations with nickel and copper materials. In industrial concerns regarding the degradation of mechanical properties of reactor materials due to irradiation-induced defects, Yabuuchi et al. employed MD simulations to unravel the relationship between dislocations and defects. Their focus was probing the interaction between edge dislocations and geometric configurations of micropores with varying surface features. The goal was to comprehend the influence of cutting mechanisms and micropores on the irradiation hardening of pure iron [40]. Furthermore, researchers have investigated the interaction between dislocations and micropores in iron, molybdenum, and binary alloys like Fe/Cu, Fe/Ni, Ni/Al, and Al/Mg, all possessing body-centered cubic crystal structures [102,135,136,173,234–243]. The quantity and mobility of dislocations surrounding micropores impact the growth rate, resulting in a faster growth rate for larger micropores, thus elucidating the observed size effect in micropores' growth. In polycrystalline materials, the factors influencing micropore growth become more complex. Micropores may exist within individual grains or at grain boundaries, and consequently, the microstructure, including grain boundaries (GBs), contributes to the evolution of micropores. In actual polycrystalline materials, micropores frequently nucleate at the junction of two adjacent GBs or multiple GBs. The features of GBs play a crucial role in influencing complex interface behaviors, such as GB slip and slip transfer, which subsequently impact mechanical properties and the evolution of micropores [244,245]. Understanding the interaction between micropores and GBs is

crucial for designing radiation-resistant materials and achieving high-quality metallurgical diffusion connections through GB engineering. Migrated GBs can exhibit diverse behaviors when interacting with micropores, such as fixation to the micropores, unhindered passage through the micropores, or complete dissolution of the micropores [226]. MD simulations indicate that higher temperatures significantly enhance the dissolution capability of high-angle GBs toward micropores. Studies on the interaction between cracks and micropores reveal that the propagation behavior of cracks is easily influenced by the distribution of micropores [96]. Moreover, a single micropore at the crack tip can impact the direction and velocity of crack propagation through interactions with the micropores. In a related study, Cui et al. investigated the interaction of shock waves with pre-existing nano micropores and the role of shear stress in iron phase transitions [227]. Nanopores were identified as preferred nucleation sites for iron phase transitions, accelerating the growth of the transition region. Additionally, the presence of micropores lowered the threshold pressure and increased the nucleation rate, facilitating the formation and growth of the new phase. The results also suggested that the size of the micropores influenced the phase transition process. Considering the intricate microstructure of nickel-based single-crystal superalloys employed in aero-engine turbine blades, Yang et al. developed Ni, Ni_3Al, and Ni/Ni_3Al interface models to assess the expansion dynamics of micropores within these three distinct microstructure configurations [221]. The author has similarly conducted research, employing tensile MD simulations to investigate the evolutionary behavior of columnar pores within the aforementioned diverse microstructure matrix models (Figure 19) [187]. Additionally, Cui et al. explored the impact of micropores on the deformation mechanism of nickel-based single-crystal superalloys by analyzing the interaction between dislocations and strengthening phases. Their investigation revealed that defects, such as micropores, can lower the difficulty of dislocation penetration into the strengthening phase, consequently diminishing the strengthening effect and resulting in a decline in the mechanical properties of nickel-based single-crystal superalloys [227]. The above findings indicate significant advancements in research related to the interaction between micropores and microstructures or the evolution of microstructures considering the influence of micropores, especially in the nuclear industry. This progress is evident in understanding the mechanical properties of nuclear reactor materials and the design and development of materials for radiation damage deformation, such as advanced aero-engine blade materials like superalloys. As more advanced materials and specialized porous materials are developed, the impact of micropores is gaining increased attention from researchers. MD simulations of interactions between micropores and microstructure evolution are gradually expanding to more demanding environments (thermal–mechanical–electrical coupling), achieving higher precision (micro–nano machining and micro–nano manufacturing), deeper levels (unified theoretical frameworks), and larger scales (spatiotemporal consistency calculations aligning with experimental conditions).

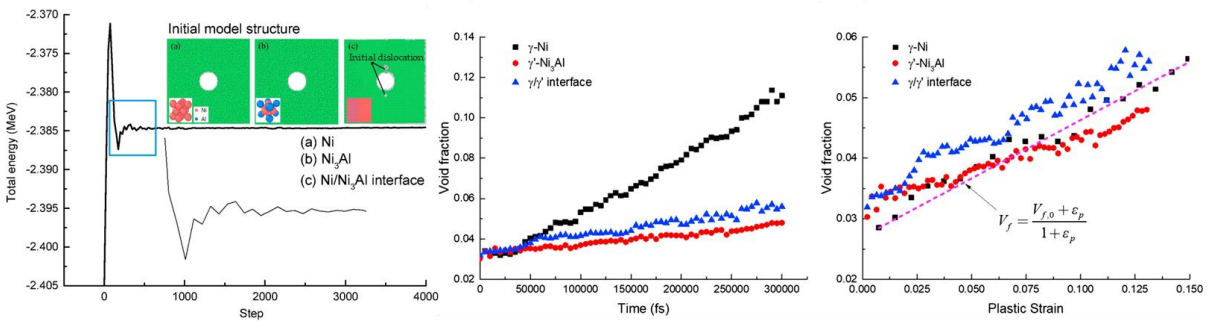

Figure 19. Atomic simulation of the effect of micropore location on micropore growth [187]. (**a**) Simulation of the system relaxation to equilibrium state; (**b**) the microstructure of the model after relaxation evolution of the volume fraction of micropore. Reprinted with permission from ref. [187]; 2019 Computational Materials Science.

8. Discussion and Outlook

Micropores are the primary sources of crack initiation in material damage and failure. Their presence poses significant safety risks during service, as the evolution of micropores in service conditions exhibits complex 3D features such as morphology, size, and distribution. This rapidly leads to the degradation of the surrounding tissue and nucleation of cracks, resulting in significant performance discrepancies and severely constraining the application of metal materials. Therefore, a clear understanding of the influence of micropore evolution on material performance is an essential aspect of the continuous development of metal materials.

At present, research on micropore evolution is predominantly centered on the growth and coalescence of micropores, considering various influencing factors such as stress state, porosity, dislocations, crystal orientation, and initial pore shape, with relatively limited investigations into micropore nucleation, collapse, inter-pore interactions, and the influence of micropores on other microstructural features. Nucleation represents the initial stage of micropore evolution, typically occurring at the microscale. However, our understanding of nucleation mechanisms is restricted due to the immaturity of current observation techniques. Similarly, the collapse process is often rapid, especially at the microscale, making direct observation and measurement challenging through experimental methods.

In situ XCT allows for the simultaneous and continuous observation of micropore evolution during experiments, but it may come with higher costs. Relying solely on experimental observations is insufficient to analyze micropore evolution and damage effects comprehensively. Advanced numerical simulation methods like DD and MD are used to understand micropore evolution mechanisms. By combining the strengths of DD and MD, CPFEM can effectively predict microstructure deformation damage in metallic materials and establish the relationship between microstructure and macroscopic properties. Incorporating pore evolution models such as the Gurson model and its extensions into crystal plasticity models allows for considering pore evolution within the crystal plasticity framework. This comprehensive multiscale approach is crucial for studying micropores' plastic behavior and evolution mechanisms.

The Gurson model is a classic model in research on the growth of pores. It is widely used to study the evolution of pores in materials. Since then, numerous scholars have expanded upon it, resulting in theoretical models such as GTN, LPD, and GLD. These theoretical models consider various factors, including different stress states, the influence of micropore nucleation, pore shape, and temperature impact, making them applicable under different conditions. The study of material damage using models like Gurson, GTN, LPD, and GLD has dramatically facilitated research by making assumptions about certain material characteristics. However, these assumptions also limit the ability of such studies to consider all influencing factors in real-world scenarios simultaneously. Each model can only investigate pore evolution under specific conditions. Future developments in this field should focus on incorporating more influencing factors and improving the descriptive capabilities of the models. Furthermore, applying these models to more complex pore morphologies and material systems is necessary to enhance their accuracy and applicability.

Indeed, with the growing demands across various application fields, understanding and controlling the evolution of micropores is becoming increasingly crucial. Integrating advanced observation and characterization techniques with sophisticated numerical methods provides more experimental data and theoretical support for an in-depth exploration of the relationship between micropores and material properties. This integration allows for optimizing material performance, enhancing mechanical strength, electrical and thermal conductivity, and accurate material lifespan and degradation predictions. This, in turn, ensures the reliability, durability, and expansion of application domains for materials. Furthermore, a thorough investigation into micropores' formation and evolution mechanisms offers more precise guidance for the design and fabrication of advanced materials. By exerting control over the distribution, morphology, and size of micropores, it becomes

possible to enhance the performance and functionality of materials, thereby propelling the advancement of advanced materials.

In conclusion, the evolution of micropores leads to the degradation of the surrounding area and the nucleation of cracks, which limits the application of advanced metal materials. The evolution process occurs at the microscale, making direct observation and measurement through SEM, TEM, and XCT challenging. Advanced numerical simulation methods such as DD and MD have been employed to understand the evolutionary mechanism of micropores. Combined with CPFEM, the deformation and damage of the microstructure of metal materials can be effectively predicted, and the relationship between microstructure and macroscopic performance can be established.

Incorporating theoretical models such as the Gurson model and its extensions into crystal plasticity finite element models allows for discussing micropore evolution processes within the framework of crystal plasticity theory, providing great convenience for related research. However, the Gurson model and its extensions only include partial material parameters such as porosity and pore shape factor, which limits the ability to consider all influencing factors in the real world simultaneously. Additionally, these parameters are difficult to accurately measure through experiments, resulting in significant adverse effects on the model's accuracy. Therefore, each model can only investigate the evolution of micropores under specific conditions. Future developments should focus on incorporating more influential factors and improving the descriptive capabilities of the models. Additionally, these models need to be applied to more complex pore morphologies and material systems to improve accuracy and applicability. Advanced observation and characterization techniques and sophisticated numerical methods will provide more experimental data and theoretical support to explore the relationship between micropores and material properties further.

Author Contributions: Conceptualization, J.L. and J.W.; methodology, J.W.; formal analysis, J.W. and M.Z.; writing—original draft preparation, J.W. and M.Z.; writing—review and editing, J.W. and Y.P. All authors have read and agreed to the published version of the manuscript.

Funding: The research was supported by National Natural Science Foundation of China (12302105, 52305163, 52075471), Hebei Natural Science Foundation (E2022203101), Funded by Science and Technology Project of Hebei Education Department (QN2023021), and The Foundation for Innovative Research Groups of the Natural Science Foundation of Hebei Province (No. E2021203011).

Data Availability Statement: No new data were created or analyzed in this study. Data sharing is not applicable to this article.

Conflicts of Interest: The authors declare no conflicts of interest.

References

1. Shi, P.; Xu, W.; Fu, B.; Liu, J.; Zhang, J.; Wang, K.; Liu, X. Pore defects in a nickel-based superalloy with high Ti content. *Prog. Nat. Sci. Mater. Int.* **2022**, *32*, 456–462. [CrossRef]
2. Xu, Z.; Britton, B.; Guo, Y. Casting voids in nickel superalloy and the mechanical behaviour under room temperature tensile deformation. *Mater. Sci. Eng. A* **2021**, *806*, 140800. [CrossRef]
3. Tong, J.Y.; Feng, W.; Fu, C.; Zheng, Y.R.; Feng, Q. Microstructure damage and mechanical properties of GH4033 alloy after short-term overheating. *Acta Metall. Sin.* **2015**, *51*, 1242–1252.
4. Zhou, B. Characterization and Control of Microstructure, Properties, Porosity and Defects in High-Strength and Heat-Resistant GW63K Magnesium Alloy Casting. Ph.D. Thesis, University of Science and Technology of China, Hefei, China, 2021.
5. Hu, B.; Yu, N.; Li, D.J.; Tian, Y.X.; Zeng, X.Q. Analysis of the causes of casting hole defects in ductile iron crankshaft. *Foundry Technol.* **2019**, *40*, 1174–1177+1182.
6. Tu, J.S. Research on the Evolution of Defects in Recycled Aluminum Alloy Sheets during Stamping Forming and Methods for Improving Their Formability. Ph.D. Thesis, General Institute of Mechanical Science Research, Beijing, China, 2022.
7. Xie, Y.L. Research on the Formation Mechanism and Regulation of Internal Defects in TC4 Titanium Alloy Formed by SLM. Master's Thesis, Shenyang Aerospace University, Shenyang, China, 2022.
8. Yv, J.W.; Kang, M.D.; Liu, Y.H.; Wu, B.; Gao, H.Y.; Wang, J. Research progress on micropore defects in nickel based single crystal high-temperature alloys. *Foundry Technol.* **2018**, *39*, 2615–2619.

9. Zhao, X.B.; Liu, L.; Yang, C.B.; Zhang, L.; Li, Y.L.; Fu, H.Z. Research progress on solidification defects of nickel based single crystal high-temperature alloys. *J. Mater. Eng.* **2012**, *6*, 93–98.
10. Chang, Z.; Yang, M.; Chen, J. Experimental investigations on deformation characteristics in microstructure level during incremental forming of AA5052 sheet. *J. Mater. Process Technol.* **2021**, *291*, 117006. [CrossRef]
11. Kuji, C.; Mizutani, M.; Takenaka, K.; Shimada, K.; Konno, T.J.; Yokobori, A.T.; Kuriyagawa, T. Relationship between blanking performance and microstructure of annealed Fe-Si-B-Cr amorphous alloy sheets. *Precis. Eng.* **2023**, *82*, 33–43. [CrossRef]
12. Zhang, D.D.; Wang, X.; Lai, X.H. Study on the reheat crack sensitivity in simulated coarse-grained heat-affected zone of 7CrMoVTiB10-10 steel. *Mater. Charact.* **2023**, *196*, 112599. [CrossRef]
13. Wang, M.H.; Liang, X.K.; Ren, W.B.; Tong, S.; Sun, X.J. Effect of Mn Content on the Toughness and Plasticity of Hot Rolled High Carbon Medium Manganese Steel. *Materials* **2023**, *16*, 2299. [CrossRef]
14. Zhang, W.; Wei, Z.; Xu, H. Effect of hot isostatic pressing on the microstructure and properties of magnesium silicide–silicon carbide/aluminum alloy (AlSi7Cu2Mg) composites. *Adv. Compos. Hybrid Mater.* **2022**, *5*, 2611–2619. [CrossRef]
15. Liu, G.X.; Lin, F.R.; Yang, J.; Wang, X.F.; Zou, J.W. Significant improvement in tensile properties of an advanced PM Ni based superalloy joint by HIP treatment. *Mater. Lett.* **2022**, *327*, 133000. [CrossRef]
16. Epishin, A.I.; Nolze, G.; Alymov, M.I. Pore Morphology in Single Crystals of a Nickel-Based Superalloy After Hot Isostatic Pressing. *Metall Mater. Trans. A* **2023**, *54*, 371–379. [CrossRef]
17. Jena, P.S.M.; Tripathy, S.; Mahato, B.; Paulose, N.; Fernando, D.C.; Sahu, J.K. Role of void nucleation at primary-γ'/γ interface on strain softening of nickel base superalloy 720Li. *J. Alloys Compd.* **2023**, *958*, 170388. [CrossRef]
18. Al-Hammadi, R.A.; Zhang, R.; Cui, C.Y.; Zhou, Z.J.; Zhou, Y.Z. Effects of temperature on superplastic and fracture behaviors of a Ni-Co-based superalloy. *J. Alloys Compd.* **2023**, *958*, 170524. [CrossRef]
19. Luo, R.; Liu, Q.T.; Gao, P.; Liu, T.; Ding, H.N.; Zhang, D.; Cao, Y.; Cheng, X.N. Effect of microstructural evolution and mechanical properties of Haynes 230 superalloy during long term aging at 700 °C. *J. Alloys Compd.* **2023**, *947*, 169495. [CrossRef]
20. Wang, H.H.; Li, X.J.; Wang, Y.X.; Wang, J. Microstructural evolution and interfacial properties of explosively welded Nb/steel composite plate during post-heat treatment. *J. Mater. Res. Technol.* **2023**, *25*, 7376–7388. [CrossRef]
21. Xiao, J.H.; Yan, L.; Zhang, P.; Li, G.L.; Li, B.Y.; Zhao, T.; Wang, H.; Chen, L.J.; Wang, D. Effects of minor Ce doping on the microstructure and mechanical performances of a EH47 grade HSLA steel for ship and ocean engineering. *Mater. Charact.* **2023**, *201*, 112931. [CrossRef]
22. Yang, Z.F.; Maurey, A.; Kang, J.D.; Wilkinson, D.S. 2D and 3D characterization of pore defects in die cast AM60. *Mater. Charact.* **2016**, *114*, 254–262. [CrossRef]
23. Gustafson, S.; Ludwig, W.; Shade, P.; Naragani, D.; Pagan, D.; Cook, P.; Yildirim, C.; Detlefs, C.; Sangid, M.D. Quantifying microscale drivers for fatigue failure via coupled synchrotron X-ray characterization and simulations. *Nat. Commun.* **2020**, *11*, 3189. [CrossRef]
24. Zhao, Y.L.; Wang, Z.; Zhang, C.; Zhang, W.W. Synchrotron X-ray tomography investigation of 3D morphologies of intermetallic phases and pores and their effect on the mechanical properties of cast Al-Cu alloys. *J. Alloys. Compd.* **2019**, *777*, 1054–1065. [CrossRef]
25. Naresh, K.; Salem, A.; Khan, K.A.; Cantwell, W.J.; Umer, R. Thermo-Mechanical Compaction-Creep and Void Analysis of Prepregs Using XCT-Aided Geometrical Models. *Appl. Compos. Mater.* **2021**, *28*, 659–684. [CrossRef]
26. Alahmed, N.; Naresh, K.; Khan, K.A.; Cantwell, W.J.; Umer, R. In-situ X-ray computed tomography characterization of compaction-creep-recovery response and statistical void analysis of carbon/epoxy prepregs. *Compos. Commun.* **2022**, *31*, 101117. [CrossRef]
27. Sundar, V.; Snow, Z.; Keist, J.; Jones, G.; Reed, R.; Reutzel, E. Flaw Identification in Additively Manufactured Parts Using X-ray Computed Tomography and Destructive Serial Sectioning. *J. Mater. Eng. Perform.* **2021**, *30*, 4958–4964. [CrossRef]
28. Lifton, J.; Liu, T. An adaptive thresholding algorithm for porosity measurement of additively manufactured metal test samples via X-ray computed tomography. *Addit. Manuf.* **2021**, *39*, 101899. [CrossRef]
29. Huang, R.X.; Zhao, T.C.; Li, H.G.; Li, P.F.; Liu, T. Preparation, compression behavior and 3D damage evolution of epoxy syntactic foam with nickel hollow spheres. *Compos. Commun.* **2022**, *29*, 101009. [CrossRef]
30. Vasilev, E.; Knezevic, M. Role of microstructural heterogeneities in damage formation and fracture of oligocrystalline Mg under tensile loading. *J. Mater. Sci. Eng. A* **2021**, *827*, 142096. [CrossRef]
31. Xie, J.; Zhang, R.; Liu, T.; Zhou, C.; Jia, L.J. Effect of Initial Void Shape on Void Growth of Structural Steels Based on Micromechanical RVE Models. *J. Mater. Civ. Eng.* **2022**, *34*, 04022010. [CrossRef]
32. Xu, S.; Chen, H.; Yang, Y.L.; Zhang, S.W.; Shen, J.; Li, Y.F.; Gao, K. Fatigue Damage Analysis of Aluminum Alloy 6061 Based on CT Scanning. *J. Mater. Eng. Perform.* **2023**, *32*, 5141–5149. [CrossRef]
33. Wang, M.L.; Yang, X.G.; Li, B.; Shi, D.Q.; Miao, G.L.; Guo, S.Q.; Fan, Y.S. The dominant role of defects on fatigue behaviour of a SLM Ni-based superalloy at elevated temperature. *Int. J. Fatigue* **2023**, *176*, 107894. [CrossRef]
34. Chen, J.; Magdysyuk, O.V.; Li, X.; Withers, P.J.; Yan, K. Investigation of ductile damage in dual phase steel during tensile deformation by in situ X-ray computed tomography. *Eng. Fract. Mech.* **2023**, *293*, 109711. [CrossRef]
35. Zhang, R.; Zhou, C.-F.; Chen, B.; Jia, L.-J. In-situ three-dimensional investigation on micro ductile fracture mechanism of mild steel. *Eng. Fract. Mech.* **2023**, *283*, 109219. [CrossRef]
36. Tian, X.; Zhang, H.; Xiang, M.; Cui, J. Investigations of void collapse in nanoporous Cu by molecular dynamics simulations. *AIP Adv.* **2023**, *13*, 065027. [CrossRef]

37. Wang, M.; Zhang, Y.; Jiang, S. Atomic Simulation of Crystallographic Orientation Effect on Void Shrinkage and Collapse in Single-Crystal Copper under Shock Compression. *J. Mater. Eng. Perform.* **2022**, *31*, 2991–3003. [CrossRef]
38. Li, X.; Peng, S.; Zhang, X.; Jiang, X.; Wang, Q. Microscopic and macroscopic analyses of the interaction mechanism between defect growth and dislocation emission in single-crystal aluminum. Fatigue Fract. *Eng. Mater. Struct.* **2021**, *44*, 3008–3022. [CrossRef]
39. Roach, A.M.; Xu, S.; Luscher, D.J.; Gianola, D.S.; Beyerlein, I.J. Interaction of extended dislocations with nanovoid clusters. *Int. J. Plast.* **2023**, *168*, 103684. [CrossRef]
40. Yabuuchi, K.; Suzudo, T. Interaction between an edge dislocation and faceted voids in body-centered cubic Fe. *J. Nucl. Mater.* **2023**, *574*, 154161. [CrossRef]
41. Barros de Moraes, E.A.; D'Elia, M.; Zayernouri, M. Machine learning of nonlocal micro-structural defect evolutions in crystalline materials. *Comput. Methods Appl. Mech. Eng.* **2023**, *403*, 115743. [CrossRef]
42. Yang, P.; Zhao, P. Void nucleation at dislocation boundaries aided by the synergy of multiple dislocation pile-ups. *Int. J. Plast.* **2023**, *171*, 103779. [CrossRef]
43. Pogorelko, V.V.; Mayer, A.E. Dynamic tensile fracture of iron: Molecular dynamics simulations and micromechanical model based on dislocation plasticity. *Int. J. Plast.* **2023**, *167*, 103678. [CrossRef]
44. Kedharnath, A.; Kapoor, R.; Sarkar, A. Classical molecular dynamics simulations of the deformation of metals under uniaxial monotonic loading: A review. *Comput. Struct.* **2021**, *254*, 106614. [CrossRef]
45. Hosseini, S.V.; Parvaz, H.; Heidari, M.; Vahdati, M. Molecular dynamics investigation into the effect of nano-void size on cutting parameters in copper single crystal. *Sādhanā* **2021**, *47*, 6. [CrossRef]
46. Rawat, S.; Chaturvedi, S. Evolution dynamics of voids in single crystal copper under triaxial loading condition. *Philos. Mag.* **2021**, *101*, 1119–1143. [CrossRef]
47. Rawat, S. Damage evolution in single crystal iron at high strain rate: A molecular dynamics study. *Pramana* **2021**, *95*, 93. [CrossRef]
48. Tu, R.; Wei, N.; Pei, Y.; Liu, Y.; Zhang, F.; Zhang, D. The Effect of Compression on the Void Coalescence under Strong Dynamic Loading. *Adv. Mater. Sci. Eng.* **2022**, *2022*, 9990161. [CrossRef]
49. Cheng, Z.; Wang, H.; Liu, G.-R.; Li, G. Molecular Dynamics Simulation of Crack Growth in Mono-Crystal Nickel with Voids and Inclusions. *Int. J. Comput. Methods* **2022**, *19*, 2250026. [CrossRef]
50. Song, W.; Yu, Y.; Guan, Y. Role of void shape on shock responses of nanoporous metallic glasses via molecular dynamics simulation. *Int. J. Mech. Sci.* **2022**, *218*, 107076. [CrossRef]
51. Qi, Z.; Wang, F.; Zeng, X.; He, L.; Wang, J.; Yang, X.; Wang, Y. Coupling Between Ductile Damage Evolution and Phase Transition in Single Crystal Niobium Subjected to High Strain Rate Loading. *J. Mater. Eng. Perform.* **2022**, *31*, 9097–9109. [CrossRef]
52. Liu, Y.-c.; Liang, Y.-c.; Zhou, L.-l.; Gao, T.-h.; Chen, Q.; Tian, Z.-a. Strengthening mechanism of Ni–Cu nanotwins with void under different tensile directions based on Molecular Dynamics simulation. *Phys. B* **2023**, *668*, 415259. [CrossRef]
53. Bhatia, M.A.; Solanki, K.N.; Moitra, A.; Tschopp, M.A. Investigating Damage Evolution at the Nanoscale: Molecular Dynamics Simulations of Nanovoid Growth in Single-Crystal Aluminum. *Metall. Mater. Trans. A Phys. Metall. Mater. Sci.* **2013**, *44A*, 617–626. [CrossRef]
54. Tang, F.L.; Cai, H.M.; Bao, H.W.; Xue, H.T.; Lu, W.J.; Zhu, L.; Rui, Z.Y. Molecular dynamics simulations of void growth in gamma-TiAl single crystal. *Comput. Mater. Sci.* **2014**, *84*, 232–237. [CrossRef]
55. Ogosi, E.; Siddiq, A.; Christie, P.; Asim, U.B.; Kartal, M.E. Mesoscale Model for Predicting Hydrogen Damage in Face Centred Cubic Crystals. *Phys. Mesomech.* **2021**, *24*, 588–597. [CrossRef]
56. Revil-Baudard, B. Effects of anisotropy on dynamic void collapse and temperature rise in low-symmetry crystals. *Mech. Res. Commun.* **2022**, *124*, 103931. [CrossRef]
57. Khavasad, P.H.; Keralavarma, S.M. Size-dependent yield criterion for single crystals containing spherical voids. *Int. J. Solids Struct.* **2023**, *283*, 112478. [CrossRef]
58. Yalçinkaya, T.; Çakmak, S.O.; Tekoğlu, C. A crystal plasticity based finite element framework for RVE calculations of two-phase materials: Void nucleation in dual-phase steels. *Finite Elem. Anal. Des.* **2021**, *187*, 103510. [CrossRef]
59. Virupakshi, S.; Kowalczyk-Gajewska, K. Cylindrical void growth vs. grain fragmentation in FCC single crystals: CPFEM study for two types of loading conditions. *Int. J. Solids Struct.* **2023**, *280*, 112397. [CrossRef]
60. Frodal, B.H.; Thomesen, S.; Børvik, T.; Hopperstad, O.S. On the coupling of damage and single crystal plasticity for ductile polycrystalline materials. *Int. J. Plast.* **2021**, *142*, 102996. [CrossRef]
61. Christodoulou, P.G.; Dancette, S.; Lebensohn, R.A.; Maire, E.; Beyerlein, I.J. Role of crystallographic orientation on intragranular void growth in polycrystalline FCC materials. *Int. J. Plast.* **2021**, *147*, 103104. [CrossRef]
62. Usman, M.; Waheed, S.; Mubashar, A. Effect of shape on void growth: A coupled Extended Finite Element Method (XFEM) and Discrete Dislocation Plasticity (DDP) study. *Eur. J. Mech. A Solids* **2022**, *92*, 104471. [CrossRef]
63. Dakshinamurthy, M.; Kowalczyk-Gajewska, K.; Vadillo, G. Influence of crystallographic orientation on the void growth at the grain boundaries in bi-crystals. *Int. J. Solids Struct.* **2021**, *212*, 61–79. [CrossRef]
64. Wciślik, W.; Lipiec, S. Voids Development in Metals: Numerical Modelling. *Materials* **2023**, *16*, 4998. [CrossRef] [PubMed]
65. Niu, L.; Zhang, Q.; Ma, Y.; Chen, Y.; Han, B.; Huang, K. A ductile fracture criterion under warm-working conditions based on the multiscale model combining molecular dynamics with finite element methods. *Int. J. Plast.* **2022**, *149*, 103185. [CrossRef]
66. Pathak, N.; Adrien, J.; Butcher, C.; Maire, E.; Worswick, M. Experimental stress state-dependent void nucleation behavior for advanced high strength steels. *Int. J. Mech. Sci.* **2020**, *179*, 105661. [CrossRef]

67. Barsoum, I.; Faleskog, J. Rupture mechanisms in combined tension and shear—Experiments. *Int. J. Solids Struct.* **2007**, *44*, 1768–1786. [CrossRef]
68. Hill, R. (Ed.) Plastic Anisotropy. In *The Mathematical Theory Of Plasticity*; Oxford University Press: Oxford, UK, 1998.
69. Bishop, R.F.; Hill, R.; Mott, N.F. The theory of indentation and hardness tests. *Proc. Phys. Soc.* **1945**, *57*, 147–159. [CrossRef]
70. Lloyd, J.T.; Matejunas, A.J.; Becker, R.; Walter, T.R.; Priddy, M.W.; Kimberley, J. Dynamic tensile failure of rolled magnesium: Simulations and experiments quantifying the role of texture and second-phase particles. *Int. J. Plast.* **2019**, *114*, 174–195. [CrossRef]
71. Liu, Y.; Chen, J.S.; Dong, X.H. A particle debonding model considering interface nanoscale damage effect. *Model. Simul. Mater. Sci. Eng.* **2021**, *29*, 015007. [CrossRef]
72. Azghandi, S.H.M.; Weiss, M.; Arhatari, B.D.; Barnett, M.R. Grain size and void formation in Mg alloy AZ31. *J. Alloys Compd.* **2020**, *816*, 152618. [CrossRef]
73. Wcislik, W.; Lipiec, S. Void-Induced Ductile Fracture of Metals: Experimental Observations. *Materials* **2022**, *15*, 6473. [CrossRef]
74. Xu, D.F.; Chen, K.H.; Chen, Y.Q.; Chen, S.Y. Evolution of the Second-Phase Particles and Their Effect on Tensile Fracture Behavior of 2219 Al-xCu Alloys. *Metals* **2020**, *10*, 197. [CrossRef]
75. Samei, J.; Sadeghi, A.; Mortezapour, H.; Salavati, S.; Amirmaleki, M.; Pekguleryuz, M.; Wilkinson, D.S. 4D X-ray tomography characterization of void nucleation and growth during deformation of strontium-added AZ31 alloys. *J. Mater. Sci. Eng. A* **2020**, *797*, 140081. [CrossRef]
76. Tekoglu, C.; Nielsen, K.L. Effect of damage-related microstructural parameters on plate tearing at steady state. *J. Mec. Theor. Appl.* **2019**, *77*, 103818. [CrossRef]
77. Guo, Y.; Paramatmuni, C.; Avcu, E. Void Nucleation and Growth from Heterophases and the Exploitation of New Toughening Mechanisms in Metals. *Crystals* **2023**, *13*, 860. [CrossRef]
78. Gregoire, M.; Brillet, H.; Vannier, P. Stress-void nucleation induced by local delaminations at Cu/Ta interfaces. In *Advanced Metallization Conference 2007 (AMC 2007): Volume 23*; Springer Nature: Berlin/Heidelberg, Germany, 2007; pp. 679–685.
79. Hu, L.L.; Zhou, J.Q. Void evolution in nanocrystalline metal film under uniform tensile stress. *J. Mater. Sci. Eng. A* **2011**, *528*, 860–867. [CrossRef]
80. Jin, C.; Shi, C.Y.; Li, G.L.; Niu, J.T. Numerical Investigation on Void Nucleation around Inclusions under Combined Mechanical and Thermal Cycling Conditions. In *Physical and Numerical Simulation of Materials Processing VII*; Trans Tech Publications Ltd.: Brooklyn, NY, USA, 2013; Volume 762, pp. 343–348.
81. Gao, B.; Li, Y.; Guo, T.F.; Guo, X.; Tang, S. Void nucleation in alloys with lamella particles under biaxial loadings. *Extrem. Mech. Lett.* **2018**, *22*, 42–50. [CrossRef]
82. Weertman, J. Zener–Stroh crack, Zener–Hollomon parameter, and other topics. *J. Appl. Phys.* **1986**, *60*, 1877–1887. [CrossRef]
83. Hirsch, P.B.; Silcox, J.; Smallman, R.E.; Westmacott, K.H. Dislocation loops in quenched aluminium. *Philos. Mag.* **1958**, *3*, 897–908. [CrossRef]
84. Kiritani, M. Formation of Voids and Dislocation Loops in Quenched Aluminum. *J. Phys. Soc. Jpn.* **1964**, *19*, 618–631. [CrossRef]
85. Shimomura, Y.; Yoshida, S. Heterogeneous Nucleation of Voids in Quenched Aluminum. *J. Phys. Soc. Jpn.* **1967**, *22*, 319–331. [CrossRef]
86. Epperson, J.E.; Gerstenberg, K.W.; Berner, D.; Kostorz, G.; Ortiz, C. Voids formed in quenched and annealed NiAl. *Philos. Mag. A* **1978**, *38*, 529–541. [CrossRef]
87. Seydel, O.; Frohberg, G.; Wever, H. Quenching-in of vacancies in pure α-iron. *Phys. Status Solidi (A)* **1994**, *144*, 69–79. [CrossRef]
88. Li, C.; Yang, K.; Gao, Y.; Wang, L. Dislocation-dominated void nucleation in shock-spalled single crystal copper: Mechanism and anisotropy. *Int. J. Plast.* **2022**, *155*, 103331. [CrossRef]
89. Noell, P.J.; Sills, R.B.; Benzerga, A.A.; Boyce, B.L. Void nucleation during ductile rupture of metals: A review. *Prog. Mater. Sci.* **2023**, *135*, 101085. [CrossRef]
90. Zhao, K.; He, J.; Ringdalen, I.G.; Zhang, Z. Effect of amorphization-mediated plasticity on the hydrogen-void interaction in ideal lattices under hydrostatic tension. *J. Appl. Phys.* **2018**, *123*, 245101. [CrossRef]
91. Yang, X.; Zeng, X.; Wang, J.; Wang, J.; Wang, F.; Ding, J. Atomic-scale modeling of the void nucleation, growth, and coalescence in Al at high strain rates. *Mech. Mater.* **2019**, *135*, 98–113. [CrossRef]
92. Liu, X.; Yan, S.; Rasmussen, K.J.R.; Deierlein, G.G. Verification of void growth-based exponential damage function for ductile crack initiation over the full range of stress triaxialities. *Eng. Fract. Mech.* **2022**, *269*, 108571. [CrossRef]
93. Wu, H.; Zhuang, X.; Zhang, W.; Zhao, Z. Anisotropic Gurson–Tvergaard–Needleman model considering the anisotropic void behaviors. *Int. J. Mech. Sci.* **2023**, *248*, 108229. [CrossRef]
94. Bonora, N.; Testa, G. Plasticity damage self-consistent model incorporating stress triaxiality and shear controlled fracture mechanisms—Model formulation. *Eng. Fract. Mech.* **2022**, *271*, 108634. [CrossRef]
95. Kusche, C.F.; Pütz, F.; Münstermann, S.; Al-Samman, T.; Korte-Kerzel, S. On the effect of strain and triaxiality on void evolution in a heterogeneous microstructure—A statistical and single void study of damage in DP800 steel. *J. Mater. Sci. Eng. A* **2021**, *799*, 140332. [CrossRef]
96. Srivastava, A.; Needleman, A. Effect of crystal orientation on porosity evolution in a creeping single crystal. *Mech. Mater.* **2015**, *90*, 10–29. [CrossRef]
97. Zhu, J.; Liu, J.; Huang, M.; Li, Z.; Zhao, L. Investigation on intragranular and intergranular void growth and their competition in polycrystalline materials. *Int. J. Plast.* **2022**, *159*, 103472. [CrossRef]

98. Yang, X.; Lei, G.; Zhao, H.; Wang, F.; Lang, L. Molecular dynamics investigation of loading orientation effect on dynamic behaviors of void in aluminum. *Vacuum* **2023**, *211*, 111967. [CrossRef]
99. Christodoulou, P.G. Role of Crystal Orientation and Void Location on Void Growth in Polycrystalline Metals. Ph.D. Thesis, University of California, Santa Barbara, CA, USA, 2023.
100. Lim, H.; Noell, P.J.; Carroll, J.D. Crystallographic orientation dependent fracture behavior in tantalum single crystals. *Scr. Mater.* **2021**, *191*, 76–80. [CrossRef]
101. Sénac, C.; Hure, J.; Tanguy, B. Void growth yield criteria for intergranular ductile fracture. *J. Mech. Phys. Solids* **2023**, *172*, 105167. [CrossRef]
102. Chang, H.J.; Segurado, J.; Llorca, J. Three-dimensional dislocation dynamics analysis of size effects on void growth. *Scr. Mater.* **2015**, *95*, 11–14. [CrossRef]
103. Alinaghian, Y.; Asadi, M.; Weck, A. Effect of pre-strain and work hardening rate on void growth and coalescence in AA5052. *Int. J. Plast.* **2014**, *53*, 193–205. [CrossRef]
104. Krasnikov, V.S.; Mayer, A.E. Plasticity driven growth of nanovoids and strength of aluminum at high rate tension: Molecular dynamics simulations and continuum modeling. *Int. J. Plast.* **2015**, *74*, 75–91. [CrossRef]
105. Cadet, C.; Besson, J.; Flouriot, S.; Forest, S.; Kerfriden, P.; de Rancourt, V. Ductile fracture of materials with randomly distributed voids. *Int. J. Fract.* **2021**, *230*, 193–223. [CrossRef]
106. Gurson, A.L.Z. *Plastic Flow and Fracture Behavior of Ductile Materials Incorporating Void Nucleation, Growth, and Interaction*; Brown University: Providence, RI, USA, 1975.
107. Mandel, J. Contribution théorique à l'étude de l'écrouissage et des lois de l'écoulement plastique. In Proceedings of the International Congress of Applied Mechanics; Springer: Berlin/Heidelberg, Germany, 1966.
108. Hill, R. The essential structure of constitutive laws for metal composites and polycrystals. *J. Mech. Phys. Solids* **1967**, *15*, 79–95. [CrossRef]
109. Gurson, A.L. Continuum Theory of Ductile Rupture by Void Nucleation and Growth: Part I—Yield Criteria and Flow Rules for Porous Ductile Media. *J. Eng. Mater. Technol.* **1977**, *99*, 2–15. [CrossRef]
110. Tvergaard, V. Influence of voids on shear band instabilities under plane strain conditions. *Int. J. Fract.* **1981**, *17*, 389–407. [CrossRef]
111. Koplik, J.; Needleman, A. Void growth and coalescence in porous plastic solids. *Int. J. Solids Struct.* **1988**, *24*, 835–853. [CrossRef]
112. Tvergaard, V. Ductile fracture by cavity nucleation between larger voids. *J. Mech. Phys. Solids* **1982**, *30*, 265–286. [CrossRef]
113. Tvergaard, V. On localization in ductile materials containing spherical voids. *Int. J. Fract.* **1982**, *18*, 237–252. [CrossRef]
114. Tvergaard, V. Effect of yield surface curvature and void nucleation on plastic flow localization. *J. Mech. Phys. Solids* **1987**, *35*, 43–60. [CrossRef]
115. Tvergaard, V.; Needleman, A. Analysis of the cup-cone fracture in a round tensile bar. *Acta Metall.* **1984**, *32*, 157–169. [CrossRef]
116. Tvergaard, V.; Needleman, A. Effect of material rate sensitivity on failure modes in the Charpy V-notch test. *J. Mech. Phys. Solids* **1986**, *34*, 213–241. [CrossRef]
117. Hom, C.L.; McMeeking, R.M. Void Growth in Elastic-Plastic Materials. *J. Appl. Mech.* **1989**, *56*, 309–317. [CrossRef]
118. Leblond, J.B.; Perrin, G.; Devaux, J. An improved Gurson-type model for hardenable ductile metals. *Eur. J. Mech. A Solids* **1995**, *14*, 499–527.
119. Jackiewicz, J. Recent Trends in the Development of Gurson's Model. In *Recent Trends in Fracture and Damage Mechanics*; Springer International Publishing: Cham, Switzerland, 2016.
120. Gologanu, M.; Leblond, J.-B.; Devaux, J. Approximate models for ductile metals containing non-spherical voids—Case of axisymmetric prolate ellipsoidal cavities. *J. Mech. Phys. Solids* **1993**, *41*, 1723–1754. [CrossRef]
121. Castañeda, P.P.; Zaidman, M. Constitutive models for porous materials with evolving microstructure. *J. Mech. Phys. Solids* **1994**, *42*, 1459–1497. [CrossRef]
122. Gologanu, M.; Leblond, J.B.; Perrin, G.; Devaux, J. *Continuum Micromechanics*; Suquet, P., Ed.; Springer: Vienna, Austria, 1997; pp. 61–130.
123. Mear, M.E.; Hutchinson, J.W. Influence of yield surface curvature on flow localization in dilatant plasticity. *Mech. Mater.* **1985**, *4*, 395–407. [CrossRef]
124. Cazacu, O.; Revil-Baudard, B.; Chandola, N.; Kondo, D. New analytical criterion for porous solids with Tresca matrix under axisymmetric loadings. *Int. J. Solids Struct.* **2014**, *51*, 861–874. [CrossRef]
125. Potirniche, G.P.; Horstemeyer, M.F.; Wagner, G.J.; Gullett, P.M. A molecular dynamics study of void growth and coalescence in single crystal nickel. *Int. J. Plast.* **2006**, *22*, 257–278. [CrossRef]
126. Seppala, E.T.; Belak, J.; Rudd, R.E. Onset of void coalescence during dynamic fracture of ductile metals. *Phys. Rev. Lett.* **2004**, *93*, 245503. [CrossRef] [PubMed]
127. Tvergaard, V.; Vadillo, G. Influence of porosity on cavitation instability predictions for elastic-plastic solids. *Int. J. Mech. Sci.* **2007**, *49*, 210–216. [CrossRef]
128. Potirniche, G.P.; Hearndon, J.L.; Horstemeyer, M.F.; Ling, X.W. Lattice orientation effects on void growth and coalescence in fcc single crystals. *Int. J. Plast.* **2006**, *22*, 921–942. [CrossRef]
129. Farrissey, L.; Ludwig, M.; McHugh, P.E.; Schmauder, S. An atomistic study of void growth in single crystalline copper. *Comput. Mater. Sci.* **2000**, *18*, 102–117. [CrossRef]

130. Seaman, L.; Curran, D. Inertia and Temperature Effects in Void Growth. *Am. Inst. Phys.* **2002**, *620*, 607–610.
131. Holte, I.; Srivastava, A.; Martínez-Pañeda, E.; Niordson, C.F.; Nielsen, K.L. Interaction of Void Spacing and Material Size Effect on Inter-Void Flow Localization. *J. Appl. Mech.* **2021**, *88*, 021010. [CrossRef]
132. Fang, Q.H.; Li, B.; Liu, Y.W. Interaction between edge dislocations and a circular hole with surface stress. *Phys. Status Solidi (b)* **2007**, *244*, 2576–2588. [CrossRef]
133. Fang, Q.H.; Liu, Y.; Liu, Y.W.; Huang, B.Y. Dislocation emission from an elliptically blunted crack tip with surface effects. *Phys. B* **2009**, *404*, 3421–3424. [CrossRef]
134. Zeng, X.; Liu, Y.W.; Wen, P.H. Dislocation emission from nanovoid with surface effects. *Int. J. Mech. Sci.* **2012**, *61*, 65–70. [CrossRef]
135. Wang, L.; Zhou, J.Q.; Hui, D.; Zhang, S. Micromechanics model for nanovoid growth and coalescence by dislocation emission: Loading and lattice orientation effects. *Int. J. Mech. Sci.* **2014**, *79*, 168–175. [CrossRef]
136. Simar, A.; Voigt, H.J.L.; Wirth, B.D. Molecular dynamics simulations of dislocation interaction with voids in nickel. *Comput. Mater. Sci.* **2011**, *50*, 1811–1817. [CrossRef]
137. Deng, X.L.; Zhu, W.J.; Zhang, Y.L.; He, H.H.; Jing, F.Q. Configuration effect on coalescence of voids in single-crystal copper under shock loading. *Comput. Mater. Sci.* **2010**, *50*, 234–238. [CrossRef]
138. Murdoch, A.I.Z. A continuum-theory of elastic material Surfaces. *Arch. Ration. Mech. Anal.* **1975**, *57*, 291–323.
139. Liu, W.H.; Zhang, X.M.; Tang, J.G.; Du, Y. Simulation of void growth and coalescence behavior with 3D crystal plasticity theory. *Comput. Mater. Sci.* **2007**, *40*, 130–139. [CrossRef]
140. Zhu, W.J.; Song, Z.F.; Deng, X.L.; He, H.L.; Cheng, X.Y. Lattice orientation effect on the nanovoid growth in copper under shock loading. *Phys. Rev. B* **2007**, *75*, 024104. [CrossRef]
141. Ha, S.; Kim, K. Void growth and coalescence in fcc single crystals. *Int. J. Mech. Sci.* **2010**, *52*, 863–873. [CrossRef]
142. Wei, N.; Shi, A.Q.; Li, Z.H.; Ou, B.X.; Zhao, S.H.; Zhao, J.H. Effect of void size and Mg contents on plastic deformation behaviors of Al-Mg alloy with pre-existing void: Molecular dynamics study. *Chin. Phys. B* **2022**, *31*, 066203. [CrossRef]
143. Song, H.Y.; Li, S.; Zhang, Y.G.; Deng, Q.; Xu, T.H.; Li, Y.L. Atomic simulations of plastic deformation behavior of $Cu_{50}Zr_{50}$ metallic glass. *J. Non Cryst. Solids* **2017**, *471*, 312–321. [CrossRef]
144. Liang, J.W.; Peng, Y.; Zhang, W.; Wang, J.P. Creep behavior of nickel-based single crystal superalloy under gradient loading. *Eng. Fail Anal.* **2022**, *131*, 105861. [CrossRef]
145. Wu, R.H.; Zhao, Y.S.; Yin, Q.; Wang, J.P.; Ai, X.; Wen, Z.X. Atomistic simulation studies of Ni-based superalloys. *J. Alloys Compd.* **2021**, *855*, 157355. [CrossRef]
146. Wang, J.P.; Yue, Z.F.; Wen, Z.X.; Zhang, D.X.; Liu, C.Y. Orientation effects on the tensile properties of single crystal nickel with nanovoid: Atomistic simulation. *Comput. Mater. Sci.* **2017**, *132*, 116–124. [CrossRef]
147. Mishin, Y.; Farkas, D.; Mehl, M.J.; Papaconstantopoulos, D.A. Interatomic potentials for monoatomic metals from experimental data and ab initio calculations. *Phys. Rev. B* **1999**, *59*, 3393–3407. [CrossRef]
148. Stukowski, A.; Albe, K. Extracting dislocations and non-dislocation crystal defects from atomistic simulation data. *Modell. Simul. Mater. Sci. Eng.* **2010**, *18*, 085001. [CrossRef]
149. Wang, J.P.; Liang, J.W.; Zhang, D.X.; Peng, Y.; Wen, Z.X. The effect of small orientation deviation from [001] to [011] on high-temperature creep properties of nickel-based single crystal. *Int. J. Plast.* **2023**, *166*, 103648. [CrossRef]
150. Tang, Y.Z.; Bringa, E.M.; Meyers, M.A. Ductile tensile failure in metals through initiation and growth of nanosized voids. *Acta Mater.* **2012**, *60*, 4856–4865. [CrossRef]
151. Liu, J.; Yuan, S.; Li, Z.; Huang, M.; Zhao, L.; Zhu, Y. Size-dependent microvoid growth in heterogeneous polycrystals. *Int. J. Plast.* **2022**, *158*, 103410. [CrossRef]
152. Traiviratana, S.; Bringa, E.M.; Benson, D.J.; Meyers, M.A. Void growth in metals: Atomistic calculations. *Acta Mater.* **2008**, *56*, 3874–3886. [CrossRef]
153. Lubarda, V.A.; Schneider, M.S.; Kalantar, D.H.; Remington, B.A.; Meyers, M.A. Void growth by dislocation emission. *Acta Mater.* **2004**, *52*, 1397–1408. [CrossRef]
154. Marian, J.; Knap, J.; Ortiz, M. Nanovoid deformation in aluminum under simple shear. *Acta Mater.* **2005**, *53*, 2893–2900. [CrossRef]
155. Cuitiño, A.M.; Ortiz, M. Ductile fracture by vacancy condensation in f.c.c. single crystals. *Acta Mater.* **1996**, *44*, 427–436. [CrossRef]
156. Lubarda, V.A. Emission of dislocations from nanovoids under combined loading. *Int. J. Plast.* **2011**, *27*, 181–200. [CrossRef]
157. Davila, L.P.; Erhart, P.; Bringa, E.M.; Meyers, M.A.; Lubarda, V.A.; Schneider, M.S.; Becker, R.; Kumar, M. Atomistic modeling of shock-induced void collapse in copper. *Appl. Phys. Lett.* **2005**, *86*, 161902. [CrossRef]
158. Seppala, E.T.; Belak, J.; Rudd, R.E. Three-dimensional molecular dynamics simulations of void coalescence during dynamic fracture of ductile metals. *Phys. Rev. B* **2005**, *71*, 064112. [CrossRef]
159. Meyers, M.A.; Traiviratana, S.; Lubarda, V.A.; Benson, D.J.; Bringa, E.M. The role of dislocations in the growth of nanosized voids in ductile failure of metals. *JOM* **2009**, *61*, 35–41. [CrossRef]
160. Seppala, E.T.; Belak, J.; Rudd, R.E. Effect of stress triaxiality on void growth in dynamic fracture of metals: A molecular dynamics study. *Phys. Rev. B* **2004**, *69*, 134101. [CrossRef]
161. Rudd, R.E.; Belak, J.F. Void nucleation and associated plasticity in dynamic fracture of polycrystalline copper: An atomistic simulation. *Comput. Mater. Sci.* **2002**, *24*, 148–153. [CrossRef]

162. Rizzoni, R.; Livieri, P.; Tovo, R. Multiscale three-dimensional stress analysis of voids clusters for the modelling of degenerated graphite in cast iron. In Proceedings of the 49th Italian Association for Stress Analysis Conference (AIAS 2020), Rimini, Italy, 9–14 September 2021; Volume 1038.
163. Zhu, J.C.; Ben Bettaieb, M.; Abed-Meraim, F. Investigation of the competition between void coalescence and macroscopic strain localization using the periodic homogenization multiscale scheme. *J. Mech. Phys. Solids* **2020**, *143*, 104042. [CrossRef]
164. Rousselier, G. Porous plasticity revisited: Macroscopic and multiscale modeling. *Int. J. Plast.* **2021**, *136*, 102881. [CrossRef]
165. Hori, M.Z. Void collapse and void growth in crystalline solids. *J. Appl. Phys.* **1987**, *62*, 2746–2757.
166. Liu, Z.G.; Wong, W.H.; Guo, T.F. Void behaviors from low to high triaxialities: Transition from void collapse to void coalescence. *Int. J. Plast.* **2016**, *84*, 183–202. [CrossRef]
167. Agoras, M.; Castañeda, P.P. Anisotropic finite-strain models for porous viscoplastic materials with microstructure evolution. *Int. J. Solids Struct.* **2014**, *51*, 981–1002. [CrossRef]
168. Li, G.M.; Wang, Y.B.; Xiang, M.Z.; Liao, Y.; Wang, K.; Chen, J. Shock response of nanoporous magnesium by molecular dynamics simulations. *Int. J. Mech. Sci.* **2018**, *141*, 143–156. [CrossRef]
169. Neogi, A.; Mitra, N. On shock response of nano-void closed/open cell copper material: Non-equilibrium molecular dynamic simulations. *J. Appl. Phys.* **2014**, *115*, 013504. [CrossRef]
170. Wang, H.Y.; Zhu, W.J.; Deng, X.L.; Song, Z.F.; Chen, X.R. Plastic deformation of helium bubble and void in aluminum under shock loading. *Acta Phys. Sin.* **2009**, *58*, 1154–1160. [CrossRef]
171. Liao, Y.; Xiang, M.Z.; Li, G.M.; Wang, K.; Zhang, X.Y.; Chen, J. Molecular dynamics studies on energy dissipation and void collapse in graded nanoporous nickel under shock compression. *Mech. Mater.* **2018**, *126*, 13–25. [CrossRef]
172. Solanki, K.; Horstemeyer, M.F.; Baskes, M.I.; Fang, H. Multiscale study of dynamic void collapse in single crystals. *Mech. Mater.* **2005**, *37*, 317–330. [CrossRef]
173. Prasad, M.R.G.; Neogi, A.; Vajragupta, N.; Janisch, R.; Hartmaier, A. Influence of Temperature on Void Collapse in Single Crystal Nickel under Hydrostatic Compression. *Materials* **2021**, *14*, 2369. [CrossRef]
174. Guan, Y.L.; Shan, J.L.; Song, W. Molecular dynamics study on nanoscale void collapse in single crystal aluminum under 1D and 3D compressions. *Comput. Mater. Sci.* **2019**, *161*, 385–393. [CrossRef]
175. Xu, Q.; Li, W.; Zhou, J.X.; Yin, Y.J.; Nan, H.; Feng, X. Molecular dynamics study on void collapse in single crystal hcp-Ti under hydrostatic compression. *Comput. Mater. Sci.* **2020**, *171*, 109280. [CrossRef]
176. Galitskiy, S.; Mishra, A.; Dongare, A.M. Modeling shock-induced void collapse in single-crystal Ta systems at the mesoscales. *Int. J. Plast.* **2023**, *164*, 103596. [CrossRef]
177. Guan, Y.L.; Dai, L.S.; Shao, J.L.; Song, W.D. Molecular dynamics study on the nanovoid collapse and local deformation in shocked $Cu_{50}Zr_{50}$ metallic glasses. *J. Non-Cryst. Solids* **2021**, *559*, 120703. [CrossRef]
178. Chen, Z.C.; Zhang, X.Q.; Li, W.H.; Yao, X.H. Shock compression of nanoporous silicon carbide at high strain rate. *Int. J. Mech. Sci.* **2022**, *224*, 107320. [CrossRef]
179. Tvergaard, V.; Niordson, C. Nonlocal plasticity effects on interaction of different size voids. *Int. J. Plast.* **2004**, *20*, 107–120. [CrossRef]
180. Cui, Y.; Chen, Z.T. Molecular dynamics simulation of the influence of elliptical void interaction on the tensile behavior of aluminum. *Comput. Mater. Sci.* **2015**, *108*, 103–113. [CrossRef]
181. Rahman, M.A.; Butcher, C.; Chen, Z.T. Void evolution and coalescence in porous ductile materials in simple shear. *Int. J. Fract.* **2012**, *177*, 129–139. [CrossRef]
182. Tran, A.S.; Fang, T.H. Void growth and coalescence in Cu-Ta metallic glasses using molecular dynamics. *Comput. Mater. Sci.* **2019**, *168*, 144–153. [CrossRef]
183. Wen, Z.X.; Wang, J.P.; Wu, Y.W.; Zhou, K.J.; Yue, Z.F. Atomistic simulation analysis of the effects of void interaction on void growth and coalescence in a metallic system. *Curr. Appl. Phys.* **2018**, *18*, 744–751. [CrossRef]
184. Brown. Embury Microstructure and design of alloys. In Proceedings of the Third International Conference on the Strength of Metals and Alloys, Cambridge, UK, 20–25 August 1973.
185. Horstemeyer, M.F.; Matalanis, M.M.; Sieber, A.M.; Botos, M.L. Micromechanical finite element calculations of temperature and void configuration effects on void growth and coalescence. *Int. J. Plast.* **2000**, *16*, 979–1013. [CrossRef]
186. Liang, J.W.; Wang, J.P.; Wen, Z.X.; Yue, Z.F. Analysis and prediction of non-isothermal creep behavior in Ni-based single crystal superalloy. *Mater. Sci. Eng. A* **2017**, *707*, 559–566. [CrossRef]
187. Wang, J.P.; Liang, J.W.; Wen, Z.X.; Yue, Z.F. Atomic simulation of void location effect on the void growth in nickel-based single crystal. *Comput. Mater. Sci.* **2019**, *160*, 245–255. [CrossRef]
188. Wang, J.P.; Liang, J.W.; Wen, Z.X.; Yang, Y.Q.; Yue, Z.F. The inter-hole interference on creep deformation behavior of nickel-based single crystal specimen with film-cooling holes. *Int. J. Mech. Sci.* **2019**, *163*, 105090. [CrossRef]
189. Yin, Q.; Wu, R.H.; Wang, J.P.; Chen, S.Q.; Lian, Y.D.; Wen, Z.X. Elastoplastic behavior of the γ-phase in Ni-based single crystal superalloys: A molecular dynamics study considering Re and temperature effect. *Mech. Mater.* **2021**, *160*, 103989. [CrossRef]
190. Wang, J.P.; Liang, J.W.; Wen, Z.X.; Yue, Z.F. Void configuration-induced change in microstructure and deformation mechanisms of nano-porous materials. *J. Appl. Phys.* **2019**, *126*, 085106. [CrossRef]
191. Bringa, E.M.; Traiviratana, S.; Meyers, M.A. Void initiation in fcc metals: Effect of loading orientation and nanocrystalline effects. *Acta Mater.* **2010**, *58*, 4458–4477. [CrossRef]

192. McClintock, F.A. A Criterion for Ductile Fracture by the Growth of Holes. *J. Appl. Mech.* **1968**, *35*, 363–371. [CrossRef]
193. Hancock, J.W.; Mackenzie, A.C. On the mechanisms of ductile failure in high-strength steels subjected to multi-axial stress-states. *J. Mech. Phys. Solids* **1976**, *24*, 147–160. [CrossRef]
194. Budiansky, B.; Hutchinson, J.W.; Slutsky, S. *Mech Solids*; Hopkins, H.G., Sewell, M.J., Eds.; Oxford Press: Pergamon, Turkey, 1982; pp. 13–45.
195. Thomason, P.F. A Theory for Ductile Fracture by Internal Nekking of Cavities. *J. Inst. Met.* **1968**, *96*, 360–365.
196. Thomason, P.F. Ductile fracture and the stability of incompressible plasticity in the presence of microvoids. *Acta Metall.* **1981**, *29*, 763–777. [CrossRef]
197. Thomason, P.F. A three-dimensional model for ductile fracture by the growth and coalescence of microvoids. *Acta Metall.* **1985**, *33*, 1087–1095. [CrossRef]
198. Thomason, P.F. Ductile fracture by the growth and coalescence of microvoids of non-uniform size and spacing. *Acta Metall. Mater.* **1993**, *41*, 2127–2134. [CrossRef]
199. Benzerga, A.A.; Leblond, J.-B. Effective Yield Criterion Accounting for Microvoid Coalescence. *J. Appl. Mech.* **2013**, *81*, 031009. [CrossRef]
200. Bandstra, J.P.; Koss, D.A. A simulation of growth and coalescence of voids during ductile fracture. *Mater. Sci. Eng. A* **2004**, *387*, 399–403. [CrossRef]
201. Horstemeyer, M.F.; Ramaswamy, S. On Factors Affecting Localization and Void Growth in Ductile Metals: A Parametric Study. *Int. J. Damage Mech.* **2000**, *9*, 5–28. [CrossRef]
202. Pardoen, T.; Hutchinson, J.W. An extended model for void growth and coalescence. *J. Mech. Phys. Solids* **2000**, *48*, 2467–2512. [CrossRef]
203. Lebensohn, R.A.; Escobedo, J.P.; Cerreta, E.K.; Dennis-Koller, D.; Bronkhorst, C.A.; Bingert, J.F. Modeling void growth in polycrystalline materials. *Acta Mater.* **2013**, *61*, 6918–6932. [CrossRef]
204. Nemcko, M.J.; Qiao, H.; Wu, P.D.; Wilkinson, D.S. Effects of void fraction on void growth and linkage in commercially pure magnesium. *Acta Mater.* **2016**, *113*, 68–80. [CrossRef]
205. Pardoen, T.; Hutchinson, J.W. Void shape and distribution effects on coalescence in elastic-plastic solids. *MRS Online Proc. Libr. (OPL)* **1999**, *578*, 327. [CrossRef]
206. Tekoglu, C.; Hutchinson, J.W.; Pardoen, T. On localization and void coalescence as a precursor to ductile fracture. *Philos. Trans. R. Soc. A* **2015**, *373*, 20140121. [CrossRef] [PubMed]
207. Liu, W.H.; Huang, H.; Tang, J.G. FEM simulation of void coalescence in FCC crystals. *Comput. Mater. Sci.* **2010**, *50*, 411–418. [CrossRef]
208. Navas, V.M.T.; Bernacki, M.; Bouchard, P.O. Void growth and coalescence in a three-dimensional non-periodic void cluster. *Int. J. Solids Struct.* **2018**, *139*, 65–78. [CrossRef]
209. Le Roy, G.; Embury, J.D.; Edwards, G.; Ashby, M.F. A model of ductile fracture based on the nucleation and growth of voids. *Acta Metall.* **1981**, *29*, 1509–1522. [CrossRef]
210. Wen, Z.X.; Li, Z.W.; Zhang, Y.M.; Wen, S.F.; Yue, Z.F. Surface slip deformation characteristics for perforated Ni-based single crystal thin plates with square and triangular penetration patterns. *Mater. Sci. Eng. A* **2018**, *723*, 56–69. [CrossRef]
211. Pineau, A.; Benzerga, A.A.; Pardoen, T. Failure of metals I: Brittle and ductile fracture. *Acta Mater.* **2016**, *107*, 424–483. [CrossRef]
212. Benzerga, A.A.; Leblond, J.-B. *Advances in Applied Mechanics*; Aref, H., Giessen, E., Eds.; Elsevier: Amsterdam, The Netherlands, 2010; Volume 44, pp. 169–305.
213. Cox, T.B.; Low, J.R. An investigation of the plastic fracture of AISI 4340 and 18 Nickel-200 grade maraging steels. *Metall. Trans.* **1974**, *5*, 1457–1470. [CrossRef]
214. Benzerga, A. Rupture Ductile des Tôles Anisotropes. Ph.D. Dissertation, École Normale de Musique, Paris, France, 2000.
215. Rodriguez, A.K.; Ayoub, G.A.; Mansoor, B.; Benzerga, A.A. Effect of strain rate and temperature on fracture of magnesium alloy AZ31B. *Acta Mater.* **2016**, *112*, 194–208. [CrossRef]
216. Song, H.Y.; Li, S.; Deng, Q. Coupling effects of thickness and aspect ratio on deformation behavior of $Cu_{50}Zr_{50}$ metallic glass. *Comput. Mater. Sci.* **2017**, *139*, 106–114. [CrossRef]
217. Weck, A.; Wilkinson, D.S.; Maire, E.; Toda, H. Visualization by X-ray tomography of void growth and coalescence leading to fracture in model materials. *Acta Mater.* **2008**, *56*, 2919–2928. [CrossRef]
218. Benzerga, A.A.; Besson, J.; Batisse, R.; Pineau, A. Synergistic effects of plastic anisotropy and void coalescence on fracture mode in plane strain. *Modell. Simul. Mater. Sci. Eng.* **2002**, *10*, 73. [CrossRef]
219. Mi, C.W.; Buttry, D.A.; Sharma, P.; Kouris, D.A. Atomistic insights into dislocation-based mechanisms of void growth and coalescence. *J. Mech. Phys. Solids* **2011**, *59*, 1858–1871. [CrossRef]
220. Gao, T.H.; Song, H.; Wang, B.; Gao, Y.; Liu, Y.T.; Xie, Q.; Chen, Q.; Xiao, Q.Q.; Liang, Y.C. Molecular dynamics simulations of tensile response for FeNiCrCoCu high-entropy alloy with voids. *Int. J. Mech. Sci.* **2023**, *237*. [CrossRef]
221. Yang, B.; Zheng, B.L.; Hu, X.J.; Zhang, K.; Li, Y.; He, P.F.; Yue, Z.F. Atomistic simulation of nanoindentation on incipient plasticity and dislocation evolution in γ/γ' phase with interface and void. *Comput. Mater. Sci.* **2016**, *114*, 172–177. [CrossRef]
222. Wang, L.; Liu, Q.; Shen, S. Effects of void-crack interaction and void distribution on crack propagation in single crystal silicon. *Eng. Fract. Mech.* **2015**, *146*, 56–66. [CrossRef]

223. Liang, S.; Huang, M.S.; Li, Z.H. Discrete dislocation modeling on interaction between type-I blunt crack and cylindrical void in single crystals. *Int. J. Solids Struct.* **2015**, *56–57*, 209–219. [CrossRef]
224. Liu, T.X.; Groh, S. Atomistic modeling of the crack-void interaction in alpha-Fe. *Mater. Sci. Eng. A* **2014**, *609*, 255–265. [CrossRef]
225. Dou, Y.K.; Cao, H.; He, X.F.; Gao, J.; Cao, J.L.; Yang, W. Interaction mechanism of an edge dislocation with a void in Fe-Ni-Cr concentrated solid-solution alloy. *J. Alloys Compd.* **2021**, *857*, 157556. [CrossRef]
226. Zhang, L.; Shibuta, Y.; Lu, C.; Huang, X.X. Interaction between nano-voids and migrating grain boundary by molecular dynamics simulation. *Acta Mater.* **2019**, *173*, 206–224. [CrossRef]
227. Cui, C.; Gong, X.G.; Chen, L.J.; Xu, W.W.; Chen, L.J. Atomic-scale investigations on dislocation-precipitate interactions influenced by voids in Ni-based superalloys. *Int. J. Mech. Sci.* **2022**, *216*, 106945. [CrossRef]
228. Zhu, B.D.; Huang, M.S.; Li, Z.H. Atomic level simulations of interaction between edge dislocations and irradiation induced ellipsoidal voids in alpha-iron. *Nucl. Instrum. Methods Phys. Res. Sect. B* **2017**, *397*, 51–61. [CrossRef]
229. Bahramyan, M.; Mousavian, R.T.; Brabazon, D. Molecular dynamic simulation of edge dislocation-void interaction in pure Al and Al-Mg alloy. *Mater. Sci. Eng. A* **2016**, *674*, 82–90. [CrossRef]
230. Xiong, L.M.; Xu, S.Z.; McDowell, D.L.; Chen, Y.P. Concurrent atomistic-continuum simulations of dislocation-void interactions in fcc crystals. *Int. J. Plast.* **2015**, *65*, 33–42. [CrossRef]
231. Osetsky, Y.N.; Bacon, D.J. Comparison of void strengthening in fcc and bcc metals: Large-scale atomic-level modelling. *Mater. Sci. Eng. A* **2005**, *400–401*, 374–377. [CrossRef]
232. Bitzek, E.; Gumbsch, P. Dynamic aspects of dislocation motion: Atomistic simulations. *Mater. Sci. Eng. A* **2005**, *400–401*, 40–44. [CrossRef]
233. Osetsky, Y.N.; Bacon, D.J. Atomic-scale mechanisms of void hardening in bcc and fcc metals. *Philos. Mag.* **2010**, *90*, 945–961. [CrossRef]
234. Wilkerson, J.W.; Ramesh, K.T. A dynamic void growth model governed by dislocation kinetics. *J. Mech. Phys. Solids* **2014**, *70*, 262–280. [CrossRef]
235. Borovikov, V.; Mendelev, M.I. Void growth via dislocation pileup impingement on grain boundary. *Mater. Lett.* **2021**, *291*, 129542. [CrossRef]
236. Yu, N.O.; Bacon, D.J. An atomic-level model for studying the dynamics of edge dislocations in metals. *Model. Simul. Mater. Sci. Eng.* **2003**, *11*, 427.
237. Osetsky, Y.N.; Bacon, D.J. Void and precipitate strengthening in α-iron: What can we learn from atomic-level modelling? *J. Nucl. Mater.* **2003**, *323*, 268–280. [CrossRef]
238. Hafez Haghighat, S.M.; Fivel, M.C.; Fikar, J.; Schaeublin, R. Dislocation–void interaction in Fe: A comparison between molecular dynamics and dislocation dynamics. *J. Nucl. Mater.* **2009**, *386–388*, 102–105. [CrossRef]
239. Hafez Haghighat, S.M.; Fikar, J.; Schäublin, R. Effect of interatomic potential on the behavior of dislocation-defect interaction simulation in α-Fe. *J. Nucl. Mater.* **2008**, *382*, 147–153. [CrossRef]
240. Hafez Haghighat, S.M.; Schaeublin, R. Molecular dynamics modeling of cavity strengthening in irradiated iron. *J. Comput. Aided. Mater. Des.* **2007**, *14*, 191–201. [CrossRef]
241. Terentyev, D.; Bacon, D.J.; Osetsky, Y.N. Interaction of an edge dislocation with voids in α-iron modelled with different interatomic potentials. *J. Phys. Condens. Matter* **2008**, *20*, 445007. [CrossRef]
242. Schäublin, R.; Chiu, Y.L. Effect of helium on irradiation-induced hardening of iron: A simulation point of view. *J. Nucl. Mater.* **2007**, *362*, 152–160. [CrossRef]
243. Lee, H.-J.; Wirth, B.D. Molecular dynamics simulation of dislocation–void interactions in BCC Mo. *J. Nucl. Mater.* **2009**, *386–388*, 115–118. [CrossRef]
244. Zhao, J.; Wang, K.H.; Lv, L.X.; Wang, L.L.; Politis, D.J.; Liu, G. Analysing the Interaction between Microscopic Deformation, Microstructure and Void Evolution of Near-α Titanium Alloys during Non-Superplastic Hot Deformation by an Integrated Crystal Plasticity Finite Element Model. *Materials* **2021**, *15*, 294. [CrossRef]
245. Chen, H.Q.; He, S.Z.; Chen, J.; Chen, F.; Zhang, S.R.; Zhang, Y.F. Molecular dynamics simulation of nanocrack closure mechanism and interface behaviors of polycrystalline austenitic steel. *Front. Mater.* **2022**, *9*, 1007502. [CrossRef]